國立臺灣大學電機資訊學院資訊網路與多媒體研究所

碩士論文

Graduate Institute of Networking and Multimedia

College of Electrical Engineering and Computer Science

National Taiwan University

Master's Thesis

混合自動駕駛環境中 V2X 速度建議系統之成效評估：人本導向之研究

Impact Assessment of V2X Speed Advisory System in Mixed Autonomy Environment : Human-Centric Approach

林紹維

Shao-Wei Lin

指導教授: 蔡欣穆 博士

Advisor: Hsin-Mu Tsai Ph.D.

中華民國 115 年 2 月

February, 2026

doi:10.6342/NTU202600337

國立臺灣大學碩士學位論文
口試委員會審定書
MASTER'S THESIS ACCEPTANCE CERTIFICATE
NATIONAL TAIWAN UNIVERSITY

混合自動駕駛環境中 V2X 速度建議系統之成效評估：人本導向之研究

Impact Assessment of V2X Speed Advisory System in Mixed Autonomy Environment : Human-Centric Approach

本論文係 林紹維 （學號 R11944038）在國立臺灣大學資訊網路與多媒體研究所完成之碩士學位論文，於民國 115 年 1 月 26 日承下列考試委員審查通過及口試及格，特此證明。

The undersigned, appointed by the Graduate Institute of Networking and Multimedia on 26 January 2026 have examined a Master's Thesis entitled above presented by LIN, SHAO-WEI (student ID: R11944038) candidate and hereby certify that it is worthy of acceptance.

口試委員 Oral examination committee:

蔡欣穆 （指導教授 Advisor）　　林靖茹　　陳柏華

系（所）主管 Director: 鄭卜壬

國立臺灣大學碩士學位論文
口試委員會審定書
MASTER'S THESIS ACCEPTANCE CERTIFICATE
NATIONAL TAIWAN UNIVERSITY

混合自動駕駛環境中 V2X 速度建議系統之成效評估：人本導向之研究

Impact Assessment of V2X Speed Advisory System in Mixed Autonomy Environment : Human-Centric Approach

本論文係 林紹維 （學號 R11944038）在國立臺灣大學資訊網路與多媒體研究所完成之碩士學位論文，於民國 115 年 1 月 26 日承下列考試委員審查通過及口試及格，特此證明。

The undersigned, appointed by the Graduate Institute of Networking and Multimedia on 26 January 2026 have examined a Master's Thesis entitled above presented by LIN, SHAO-WEI (student ID: R11944038) candidate and hereby certify that it is worthy of acceptance.

口試委員 Oral examination committee:

	林志緯	
（指導教授 Advisor）		

系（所）主管 Director: 鄭卜壬

誌謝

由衷感謝我的指導教授，蔡欣穆老師，總是耐心指導研究方向，並在我遇到困難時，提出許多珍貴的建議。和老師研究的這幾年，學會了如何深入探索一個主題，以及身為一個研究員應該注意到哪些細節及面向。在進行論文編修及製作口試投影片的過程中，更了解到有哪些微小的細節是值得注意的，並學會如何清楚地說明想傳達的重點與內容。

也感謝實驗室的大家，特別是同屆的昱廷、以峰、懷平還有家妤。雖然我們的研究都是不同的面向，但還是能共同分享在研究時遇到的心情，在漫長的研究過程中，不僅能分憂，更帶來許多歡樂。

最後，也感謝我的家人與女友一直以來的支持陪伴，總是在我憂慮的時候給予默默的支持；在研究遇到不順利的低谷時，謝謝你們用理解與包容的心態陪伴我度過，讓我最終能順利地完成學業。

doi:10.6342/NTU202600337

摘要

高速公路的交通流經常因「幽靈塞車 (Phantom Jams)」而陷入不穩定，此現象主要源於人類駕駛的反應延遲。儘管聯網自駕車 (CAVs) 被廣泛視為解決此問題的終極方案，但受限於混合自動駕駛環境的複雜性與法律規範，其全面部署仍難以在短期內實現。為解決此過渡期缺口，本研究提出一套速度建議系統 (SAS)，透過 V2X 通訊技術賦予人類駕駛車輛 (HDVs) 前瞻性的預判能力。

鑑於現有標準模型無法重現導致交通震盪的特定人類駕駛失誤，本研究首先在 SUMO 模擬環境中開發了一套「以人為本跟車模型 (HCCFM)」。該架構明確納入了人類駕駛固有的生理與心理限制——具體整合了韋伯定律 (Weber's Law) 與非對稱風險感知——以精確重現真實的駕駛動態。

實驗結果證實，SAS 發揮了強大的「消波 (Wave-Breaker)」作用，將震盪波傳播距離減少了 94.9%，並將總延遲時間降低了 90.4%。在巨觀層面上，該系統在瓶頸場景中使道路容量提升了 21.2%。敏感度分析顯示，效率顯著提升的關鍵規模 (Critical Mass) 位於 50% 的市場滲透率。關鍵的是，穩健性測試證實即便在 50% 封包遺失率下，系統運作效率仍優於純人類駕駛；且其失效安全機制確保了即使在 100% 通訊中斷的情況下，仍能維持零碰撞紀錄。

關鍵字：混合自動駕駛、V2X、交通震盪緩解、跟車模型、SUMO 模擬、速度建議系統 (SAS)

doi:10.6342/NTU202600337

Abstract

Highway traffic is frequently destabilized by "phantom jams" driven by human reaction latency. While Connected and Autonomous Vehicles (CAVs) are widely proposed as the ultimate solution, their immediate deployment is constrained by the complexities of mixed autonomy and legal regulations. To address this gap, we propose a Speed Advisory System (SAS) that empowers Human-Driven Vehicles (HDVs) with V2X-enabled foresight. Since standard models fail to replicate the specific human errors that propagate these instabilities, we first develop a Human-Centric Car-Following Model (HCCFM) within SUMO. This framework explicitly accounts for the innate physiological and psychological constraints of human drivers—specifically integrating Weber's Law and asymmetric risk perception—to accurately reproduce realistic driving dynamics. Experimental results demonstrate that the SAS acts as a strong "wave-breaker," reducing shockwave propagation distance by 94.9% and total delay by 90.4%. Macroscopically, the system increases the capacity by 21.2% in the bottleneck scenarios. Sensitivity analysis reveals a critical

doi:10.6342/NTU202600337

mass at 50% penetration for efficiency gains. In particular, robustness tests confirm that the system remains more efficient than human driving even under 50% packet loss, and the fail-safe mechanism ensures zero collisions even under 100% communication failure.

Keywords:Mixed Autonomy, V2X Communication, Speed Advisory System(SAS), Car-Following Model, Traffic Shockwaves, Human-Centric Design.

doi:10.6342/NTU202600337

Contents

doi:10.6342/NTU202600337

doi:10.6342/NTU202600337

doi:10.6342/NTU202600337

doi:10.6342/NTU202600337

List of Figures

doi:10.6342/NTU202600337

doi:10.6342/NTU202600337

doi:10.6342/NTU202600337

List of Tables

doi:10.6342/NTU202600337

Chapter 1

Introduction

1.1 Background and Motivation

In recent decades, the rapid growth of vehicular traffic has outpaced the expansion of road infrastructure, leading to severe congestion on highways worldwide. A prominent example is the recurrent congestion on the National Highway No. 5 corridor in Taiwan, particularly during peak intercity travel periods. Traffic engineering studies have identified that a significant portion of this congestion is not caused by physical bottlenecks (such as accidents or lane closures) but by the phenomenon known as *traffic shockwaves* (or phantom traffic jams) [1].

Traffic shockwaves are typically triggered by minor disturbances, such as a driver braking abruptly. Due to the inherent reaction latency and perception errors of human drivers, following vehicles must brake harder to maintain safety, causing the disturbance to amplify as it propagates upstream. This "stop-and-go" dynamic not only degrades road capacity but also increases fuel consumption and collision risks [2].

While Connected and Autonomous Vehicles (CAVs) offer a theoretical solution to

doi:10.6342/NTU202600337

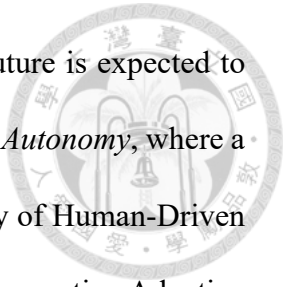

eliminate these inefficiencies, the transition to a fully autonomous future is expected to take decades. Traffic environments are evolving into a stage of *Mixed Autonomy*, where a small percentage of automated vehicles share the road with a majority of Human-Driven Vehicles (HDVs). In this transitional phase, existing solutions like Cooperative Adaptive Cruise Control (CACC) have limited impact due to low market penetration rates.

Therefore, there is an urgent need for solutions that leverage available Vehicle-to-Everything (V2X) technologies to enhance the performance of human drivers. This study focuses on Connected Human-Driven Vehicles (CHVs)—vehicles that remain under manual control but are augmented by real-time V2X information. By providing proactive speed advisories, such a system can mitigate human perception errors and reaction delays, offering a scalable pathway to stabilize traffic flow without waiting for full automation.

1.2 Problem Statement

The core problem addressed in this thesis is the *string instability* inherent in human-dominated traffic flows. Human drivers suffer from two fundamental limitations:

1. **Reaction Latency:** The time delay between perceiving a stimulus (e.g., brake lights) and executing an action.
2. **Perception Error:** The inaccuracy in the relative distance and speed estimation performed by human drivers, often described by Weber's Law.

Existing microscopic simulation models such as the standard Krauss model in SUMO [3] often simplify these human factors, leading to an inability to accurately replicate the formation of shockwaves. Furthermore, current Advanced Driver Assistance Systems

doi:10.6342/NTU202600337

(ADAS) mainly focus on safety (collision avoidance) rather than flow efficiency. One key reason is the lack of deployment of V2X communication technologies in current vehicle products. To be able to dampen the shockwave, such communications among nearby vehicles in the same lane is crucial.

1.3 Proposed Solution

To address these challenges, this thesis proposes an **Speed Advisory System (SAS)**. The SAS is a "Human-in-the-Loop" cooperative system that utilizes V2X communication to look ahead of the immediate traffic. Instead of taking over control, it provides preemptive kinematic advisories (acceleration/deceleration suggestions) to the driver. By alerting the driver to downstream disturbances before they are visually perceptible, the system effectively reduces the aggregate reaction time and smooths out the braking trajectory.

To rigorously evaluate this system, we also develop a novel **Human-Centric Car-Following Model (HCCFM)**. Unlike traditional models, the HCCFM incorporates distance-dependent estimation errors based on Weber's Law and asymmetric risk perception, ensuring that the simulation environment accurately reflects the instability of real-world mixed traffic.

1.4 Thesis Contributions

The main contributions of this thesis are summarized as follows:

1. **Development of a Human-Centric Car-Following Model (HCCFM):** We formulated a stochastic driver model that integrates variable reaction times and perception

doi:10.6342/NTU202600337

errors governed by Weber's Law. The model was rigorously calibrated against the NGSIM trajectory dataset to reproduce realistic stop-and-go behaviors.

2. **Design of the Speed Advisory System (SAS):** We designed a cooperative control logic that calculates optimal acceleration suggestions based on V2X data. Specifically, the system addresses the efficiency loss caused by the conservative mindset of human drivers, quantified as "Conservative Coefficients" (asymmetric risk perception) in our work. By providing preemptive advisories, the SAS effectively neutralizes the behavioral hysteresis found in manual driving, allowing for tighter yet safer gap management.

3. **Validation of Microscopic Stability Mechanism:** Through *pulse step* stress tests, we demonstrated that the SAS acts as a shockwave damper. The system reduced the upstream propagation distance of shockwaves by over **94%** and reduced the total delay time by approximately **90%** compared to the HDV baseline.

4. **Quantification of Macroscopic Capacity Gains:** In a *virtual bottleneck* scenario, the SAS demonstrated a capacity improvement of approximately **22% to 46%**, depending on the safety configuration.

5. **Sensitivity and Robustness Analysis:** We analyzed the system performance across varying market penetration rates, demonstrating that shockwave propagation decreases linearly with adoption, and road capacity is effectively increased at around 50% penetration rate. Furthermore, we evaluated the system robustness against network instability. Using a Gilbert-Elliot model to simulate bursty packet losses, we validated a fail-safe mechanism that ensures zero collisions and graceful performance degradation during communication blackouts.

doi:10.6342/NTU202600337

1.5 Thesis Organization

The remainder of this thesis is organized as follows: Chapter 2 reviews related work on traffic flow theory and car-following models. Chapter 3 details the system design of the HCCFM and SAS. Chapter 4 describes the implementation and calibration process in the SUMO simulator. Chapter 5 presents the comprehensive evaluation results, including microscopic stability, macroscopic capacity, and sensitivity analyses. Finally, Chapter 6 concludes the thesis and discusses future directions.

doi:10.6342/NTU202600337

Chapter 2

Related Work

2.1 Traffic Shockwave Mitigation in Mixed Autonomy

To address the traffic instabilities and congestion issues highlighted in Chapter 1, traffic management strategies have evolved significantly from macroscopic infrastructure controls to microscopic vehicular automation.

Historically, infrastructure-based strategies were the primary means of flow control. **Variable Speed Limits (VSL)** and **Ramp Metering (RM)** have been widely adopted to homogenize traffic speeds and reduce crash risks by adjusting limits based on real-time density. The effects of VSL has been studied in many works [4, 5], while a dynamic speed limiting method has been proposed to reduce shockwaves on freeway [6]. These systems provide intuitive visual cues for driver to follow. However, such systems usually only prescribe maximum speed limits rather than adjusting vehicle velocities to a specific target speed. Additionally, this information is available only when vehicles pass fixed checkpoints, limiting the continuity of the control.

To overcome the limitations of fixed infrastructure, extensive literature has investi-

doi:10.6342/NTU202600337

gated the potential of Connected and Autonomous Vehicles (CAVs). Foundational studies confirm that introducing CAVs significantly improves string stability and throughput. Ghiasi et al. [7] and Abdulsattar et al. [8] demonstrated that highway capacity increases with CAV penetration rates. Guériau et al. [9] further quantified this, showing that while efficiency benefits are non-linear, a penetration rate between 20% and 40% often yields near-maximum flow improvements. Similarly, Sala et al. [10] showed that replacing regular traffic with AV platoons can drastically increase lane capacity due to reduced reaction times.

To actively manage these benefits, researchers have proposed various control frameworks. Wang et al. [11] proposed the Leading Cruise Control (LCC) strategy, proving that even a single CAV acting as a mobile actuator can stabilize mixed traffic flow. Liu et al. [12] developed an oscillation mitigation MPC framework to optimize longitudinal control. Furthermore, Li et al. [13] and Wu et al. [14] explored cooperative formations and reinforcement learning approaches to stabilize mixed autonomy beyond simple platooning.

However, the transition to a fully autonomous future faces significant hurdles. As noted in [15], legal frameworks, liability issues, and public acceptance currently hinder the widespread deployment of Level 4/5 AVs. In the foreseeable future, traffic will operate in a state of mixed autonomy, dominated by HDVs [16]. While Cooperative Adaptive Cruise Control (CACC) leverages V2V communication to suppress shockwaves [17], its effectiveness is often compromised by communication instability. Di Vaio et al. [18] and Garg et al. [19] emphasized that control protocols must account for packet losses and delays, which can force CAVs to degrade to standard ACC, negating their benefits.

doi:10.6342/NTU202600337

Consequently, there is an urgent need for "Human-in-the-Loop" solutions. Instead of replacing the driver, recent research proposes empowering them via V2X advisories. Nguyen et al. [20] and Wan et al. [21] proposed advisory frameworks for arterial roads. Wu et al. [22] developed a real-time speed advisory system by presenting a LED strip to the driver for acceleration and deceleration instructions, where the results demonstrate a deduction of 76.4% reaction delay and the standard deviation of the distance between two consecutive cars decreaseing by 40%. However, these systems lacks macroscopic quantification and robustness analysis against communication failures. This thesis proposes a SAS specifically designed to mitigate highway shockwaves by simplifying the human cognitive task, serving as a robust transitional solution.

2.2 Car-Following Models

To accurately evaluate the impact of such advisory systems, the underlying simulation environment must faithfully replicate the longitudinal interaction between vehicles.

Traditional models like Krauss [23] and the Intelligent Driver Model (IDM) [24] have been adapted for mixed traffic of human-driven and autonomous vehicles. Zhu et al. [25] and Alturki et al. [26] analyzed mixed flows by adjusting parameters to reflect the heterogeneity between human and autonomous driving. Sun et al. [27] utilized IDM-based controllers to analyze the link between string instability and traffic oscillations.

Despite these advancements, standard models often oversimplify human errors. Treiber et al. [28] introduced the Human Driver Model (HDM) to incorporate reaction delays and anticipation. However, as highlighted by Li et al. [29], simply adding a delay term is insufficient. Real-world instability arises from specific cognitive characteristics:

doi:10.6342/NTU202600337

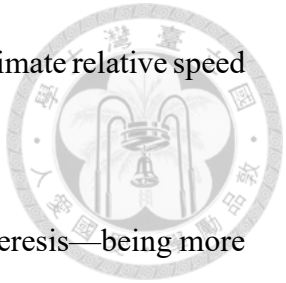

- **Distance-Dependent Perception Error:** Drivers struggle to estimate relative speed as the distance increases (Weber's Law [30]).
- **Asymmetric Risk Perception:** Drivers exhibit behavioral hysteresis—being more conservative when closing in than when falling behind [31].

Current simulations often assume perfect perception or simple white-noise errors, which fail to capture the "stop-and-go" dynamics accurately. Consequently, this study introduces the **Human-Centric Car-Following Model (HCCFM)**, which integrates these psychological factors to provide a rigorous baseline for validating the proposed SAS.

2.3 Driver Reaction Dynamics and Cognitive Load

A critical theoretical foundation for the SAS lies in the decomposition of driver reaction time (RT) and cognitive load.

As detailed by Green [32], the perception-reaction time (PRT) is not an instantaneous event but a sequence comprising sensation, perception, response selection—such as determining whether to brake, accelerate, or change lanes—and movement. In typical unassisted driving, the driver faces a **Choice Reaction Time (CRT)** task. The driver must continuously interpret ambiguous visual cues, e.g. distinguishing between a mild deceleration and an emergency brake, and select an appropriate response.

According to Hick's Law [33, 34], the time required to make a decision increases logarithmically with the number of choices. This cognitive load inherently induces significant latency, often exceeding 1.2 seconds, which acts as the primary amplifier for traffic shockwaves.

doi:10.6342/NTU202600337

The proposed SAS aims to fundamentally alter this dynamic by converting the driving task from a CRT paradigm to a **Simple Reaction Time (SRT)** paradigm. By processing V2X data to generate a difference to the target speed, such as a speed adjustment of +5 km/h, the system offloads the complex "perception" and "response selection" phases from the human driver. This theoretical reduction in cognitive load justifies the reduced effective reaction time parameter used in our system design, enabling HDVs to achieve response times comparable to semi-automated systems and effectively dampen traffic disturbances.

2.4 Research Gaps and Thesis Positioning

While existing traffic mitigation strategies such as variable speed limits or fully autonomous platooning offer theoretical solutions to congestion, they often suffer from deployment constraints including local legislation, commercial considerations, reliance on extensive infrastructure or the requirement for high market penetration rates. Consequently, current approaches struggle to effectively stabilize traffic during the transitional phase of mixed autonomy. This limitation underscores the critical need for level 2/3 human-in-the-loop solutions, specifically speed advisory systems, which empower connected HDVs to act as stabilizing agents without necessitating full automation.

Regarding microscopic simulation, standard car-following models often oversimplify human behavior by assuming perfect state perception or instantaneous reaction capabilities. These models fail to capture the specific physiological constraints that trigger phantom traffic jams in real-world scenarios. To address this deficiency, this thesis proposes HCCFM that explicitly incorporates distance-dependent perception errors governed by Weber's Law and asymmetric risk assessment known as hysteresis, thereby ensuring the simulation faithfully reproduces the instability mechanisms of mixed traffic.

doi:10.6342/NTU202600337

Furthermore, current research rarely bridges the gap between behavioral psychology and macroscopic traffic flow efficiency. This work integrates cognitive theory directly into the control loop by designing a system that facilitates the transition from high-latency choice reaction time to low-latency simple reaction time. By explicitly modeling this cognitive offloading, the thesis demonstrates how reducing the mental burden on drivers can serve as a fundamental yet effective mechanism for suppressing shockwaves and enhancing overall road capacity.

doi:10.6342/NTU202600337

Chapter 3

System Design

3.1 Overview

This chapter details the comprehensive design and implementation of the proposed SAS. We begin in Section 3.2 by defining the **System Architecture**, illustrating how 5G V2X communication and local sensing mechanisms are integrated to assist human drivers in a mixed traffic environment. Subsequently, in Section 3.3, we introduce the SUMO simulation environment and analyze the limitations of the standard Krauss car-following model. Finally, we present the proposed Human-Centric Car-Following Model (HCCFM) and the SAS control algorithms, demonstrating how the system incorporates variable human reaction times to improve traffic flow stability and road capacity.

3.2 System Architecture

This section outlines the physical architecture and communication framework designed to implement the SAS. The system utilizes a cooperative "Human-in-the-Loop" design to bridge the gap between automated data acquisition and human actuation.

doi:10.6342/NTU202600337

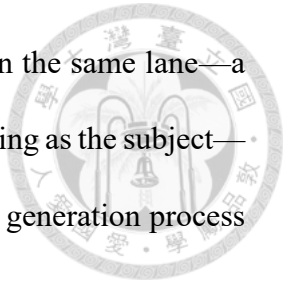

The proposed architecture comprises two consecutive vehicles in the same lane—a leading vehicle acting as the front target and a following vehicle operating as the subject—within a 5G-enabled environment. The data acquisition and advisory generation process follows a four-stage loop, as illustrated in Figure 3.1:

1. **V2N2V Communication (5G):** The leading vehicle continuously uploads its kinematic states, i.e., velocity and acceleration, sampled at 10Hz, to a cloud-based V2X application server via the 5G uplink. To identify the correct target, the following vehicle utilizes a dashboard camera to capture the license plate number of the vehicle directly in front. Using this license plate as a unique identifier, the following vehicle subscribes to the leading vehicle's data stream via the 5G downlink, ensuring that the retrieved kinematic information corresponds to the vehicle directly in front.

2. **Local Sensing (ToF via Bluetooth):** To ensure precise gap estimation, the following vehicle is equipped with a Time-of-Flight (ToF) distance sensor mounted on the front bumper. This sensor measures the physical headway $g(t)$ and transmits the reading to the driver's smartphone via a high-speed Bluetooth Low Energy (BLE) connection. While many ADAS systems do have the distance information, these are often not externally accessible, thus we design the system as a fully self-contained system.

3. **Processing Unit (Mobile App):** The SAS algorithm runs on the smartphone on the following vehicle. It fuses the leader data with the local gap data to compute the optimal advisory speed.

4. **Human-Machine Interface (Smartphone Display):** The calculated advisory speed

doi:10.6342/NTU202600337

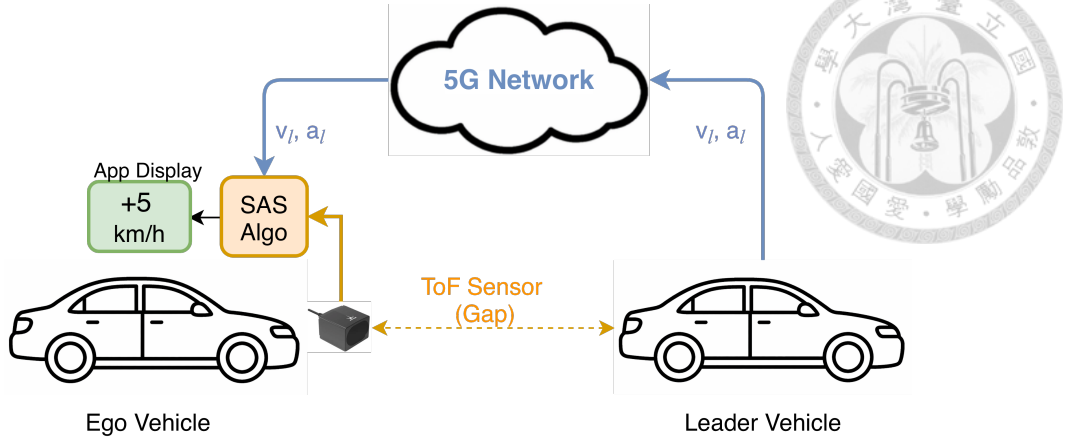

Figure 3.1: Overview of system architecture.

difference is displayed directly on the screen of the driver's smartphone application. The interface provides a clear numerical recommendation,such as a speed adjustment of +5 km/h, allowing the driver to adjust their speed promptly.

The validity of this proposed architecture relies on the ability of the experimental setup to accurately reflect real-world operational conditions, particularly regarding system latency and communication stability. According to end-to-end (E2E) latency modeling in [35], the temporal resolution of 0.1 seconds is sufficient to encapsulate 5G V2X latencies, which ranges from **4 ms to 10 ms** in MEC-based deployments, and **28 ms to 58 ms** in centralized cloud deployments. Furthermore, the evaluation is grounded in two core operational assumptions: (i) 100% compliance of the driver with speed advisories, and (ii) a traffic flow consisting exclusively of standard passenger cars, while heavy vehicles such as trucks or buses are excluded. These constraints ensure a controlled environment for assessing the efficacy of V2X-enabled foresight.

doi:10.6342/NTU202600337

3.3 SUMO Simulation Environment

To validate the proposed SAS and analyze traffic shockwave propagation, this study utilizes **Simulation of Urban MObility (SUMO)**, an open-source, microscopic, multi-modal traffic simulation package. SUMO was selected for its ability to model discrete vehicle interactions with high fidelity and its support for the **Traffic Control Interface (TraCI)**. TraCI allows for real-time retrieval and manipulation of vehicle states including position, speed and acceleration via external Python scripts, enabling the implementation of the custom "Human-in-the-Loop" control logic and the HCCFM proposed in this thesis.

3.3.1 Temporal Resolution and Action Granularity

A critical requirement for modeling traffic instability is the precise simulation of reaction latencies. Standard macroscopic models or coarse-grained microscopic simulations (e.g., one-second step length) often fail to capture the high-frequency dynamics of "stop-and-go" waves.

- **Simulation Step Length (Δt):** To ensure sufficient temporal resolution, the global simulation step length is set to **0.1 seconds**. This sub-second resolution is essential for replicating the rapid deceleration events characteristic of shockwaves and allows for the precise injection of V2X advisories.
- **Action Step Length:** To mirror the continuous nature of real-world driving, the action step length is also set to **0.1 seconds**. This fine temporal resolution prevents vehicle behaviors from being artificially constrained to coarse, discrete decision points, thereby allowing maneuvers to replicate the fluidity characteristic of physical reality.

doi:10.6342/NTU202600337

3.3.2 Car-Following Parameters

The longitudinal movement of vehicles in SUMO is governed by car-following models, which calculate the safe velocity v_{safe} to prevent collisions. The behavior is primarily constrained by the following parameters:

- **Minimum Time Headway (τ):** This parameter represents the desired minimum time gap (in seconds) that a driver attempts to maintain from the rear bumper of the leading vehicle. Physically, τ is the inverse of the maximum theoretical saturation flow (Capacity $\approx 3600/\tau$). In this research, τ is a critical variable; for HDVs, it represents the safe breaking distance required by humans, whereas for SAS-equipped vehicles, it represents the optimized gap enabled by machine precision.
- **Apparent Reaction Time:** While standard models often treat reaction time as a fixed delay equal to the simulation step, this study redefines reaction time as a specific perception delays (t_{reac}), which will be mathematically formulated in the proposed HCCFM (Section 3.5).

3.4 Krauss Model

The standard car-following model in SUMO is based on the work of Krauß [23], with specific implementation details described by Erdmann and Wagner [36]. The core concept of the Krauss model is to ensure no collision occurrence; specifically, the model makes sure that the gap $g(t)$ between the rear bumper of the leader and the front bumper of the follower remains positive at all times.

doi:10.6342/NTU202600337

A safe speed v_{safe} is calculated to ensure that the vehicle can come to a complete stop without collision, even if the leading vehicle brakes abruptly. The fundamental safety constraint is given by

$$\frac{v(t)^2}{2b} + v(t) * \tau \leq \frac{V(t)^2}{2B} + g(t) \tag{3.1}$$

where $v(t)$ and $V(t)$ are the speeds of the following and leading vehicles, b and B represent the maximum deceleration capabilities of the follower and leader, and τ denotes the reaction of the driver. This is also configured in SUMO as the minimum time headway. The term $v(t) * \tau$ accounts for the distance traveled by the follower before braking begins.

Derived from Eq. 3.1, the safe speed is theoretically obtained by solving for $v(t)$. To avoid computationally expensive square-root operations during simulation, SUMO implements a rational approximation using Taylor expansion around the average speed $\overline{v(t)} = (v(t) + V(t))/2$, assuming a constant decleration $b = B$ [36].

$$v_{safe}(t) = V(t) + \frac{g(t) - V(t)\tau}{\frac{v(t)+V(t)}{2b} + \tau} \tag{3.2}$$

Finally, the speed for the next time step $v(t + \Delta t)$ is determined by taking the minimum of the desired speed constrained by the maximum acceleration a_{max} of the vehicle, the calculated safe speed, and the maximum mechanical speed of the vehicle as shown in Eq. 3.3.

$$\tilde{v} = \min\{v(t) + a_{max}\Delta t,\ v_{safe}(t),\ v_{max}\} \tag{3.3}$$

doi:10.6342/NTU202600337

To capture the stochastic nature of human driving—specifically the tendency to *dawdle* or fail to utilize the vehicle's full acceleration potential—a noise term is introduced. Since the calculated speed $\tilde{v}$ represents the maximum allowable velocity under safety and physical constraints, any stochastic deviation acts as a subtractive term to ensure safety limits are not violated

$$v(t + \Delta t) = \max\{0,\ \tilde{v} - a_{max}\Delta t \cdot \sigma \cdot \eta\} \tag{3.4}$$

where σ denotes the imperfection of throttle control from the driver (default 0.5), reflecting the magnitude of speed under-utilization, and η is a random variable drawn from the uniform distribution $\mathcal{U}[0, 1]$. This formulation ensures that human error manifests as conservative speed reduction rather than unsafe acceleration.

Limitation in Sub-Second Simulation: While the Krauss model incorporates τ to maintain a safe headway, it fundamentally assumes **perfect state awareness**. As shown in Eq. 3.2, the calculation of $v_{safe}(t)$ utilizes the exact gap $g(t)$ and leader velocity $V(t)$ from the current simulation step. When the simulation step length is set to high resolutions (e.g., $\Delta t = 0.1s$), this implies that the driver can perceive changes of the state of the leader and adjust braking strategy every 0.1 seconds.

In reality, human drivers suffer from **physiological Perception-Reaction Time (PRT)** [32]. They do not react to the traffic state at time t, but rather to the state perceived at $t - t_{reac}$. The standard Krauss model's lack of this information delay leads to an overestimation of string stability, as vehicles react "super-humanly" fast to disturbances. This discrepancy motivates the development of the HCCFM in the next section.

doi:10.6342/NTU202600337

3.5 Human-Centric Car Following Model

Standard car-following models, including the default Krauss model, operate on the assumption of instantaneous perception and perfect state estimation. To address these physiological implausibilities, this study proposes the Human-Centric Car-Following Model (HCCFM). This framework introduces a three-stage cognitive pipeline: **delayed perception**, **imperfect estimation**, and **asymmetric risk assessment**.

3.5.1 Delayed Perception

Human driving is fundamentally a Choice Reaction Time (CRT) task [32]. Drivers must continuously interpret ambiguous visual cues, such as estimating relative speeds and selecting appropriate responses. This cognitive load introduces a non-negligible latency, typically ranging from 1.0 second to 1.5 seconds, during which the vehicle continues to travel based on prior decisions.

In the HCCFM, this latency is explicitly modeled. Instead of calculating the safe speed using the current state values at time t, the driver utilizes the states perceived t_{reac} seconds ago, as illustrated in Figure 3.2. The effective input state $S_{input}(t)$ is defined as:

$$S_{input}(t) = \{g(t - t_{reac}),\ v_{leader}(t - t_{reac}),\ v_{ego}(t - t_{reac})\} \tag{3.5}$$

where t_{reac} is a stochastic variable drawn from a normal distribution $\mathcal{N}(\mu, \sigma^2)$ for each driver, centered around 1.0 second – 1.2 seconds to reflect the CRT paradigm [32]. This ensures that the simulated driver reacts to the "past reality", naturally inducing the string instability observed in real traffic.

doi:10.6342/NTU202600337

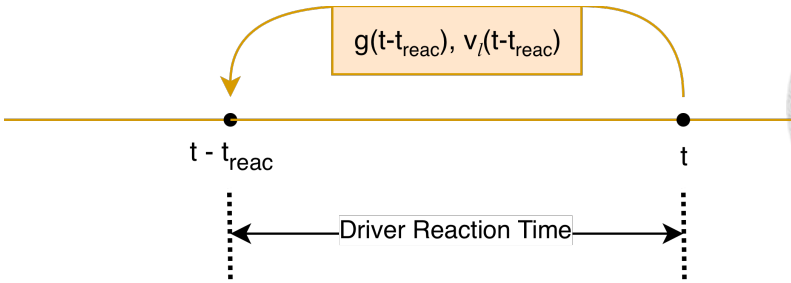

Figure 3.2: Driver reaction latency.

3.5.2 Imperfect Estimation

Human visual estimation is neither perfect nor completely random; it is distance-dependent and temporally correlated. To capture this, we integrate Weber's Law with an Ornstein-Uhlenbeck (OU) mean-reverting process [37].

The perceived gap $g_p(t)$ is modeled as the actual delayed gap distorted by an error term $E(t)$

$$g_p(t) = g(t - t_{reac}) \cdot (1 + k \cdot E(t)) \tag{3.6}$$

where k is the Weber Fraction (sensitivity coefficient, typically ≈ 0.1), and the normalized error state $E(t)$ is modeled as a discrete-time stochastic process to capture the time-correlated nature of human perception errors. Its evolution is governed by the following first-order autoregressive structure

$$E(t) = \alpha \cdot E(t - \Delta t) + \sqrt{1 - \alpha^2} \cdot \eta, \quad \eta \sim \mathcal{N}(0, 1) \tag{3.7}$$

where η is a Gaussian white noise term representing the stochastic disturbance in perception at each time step. The coefficient $\alpha = \exp(-\Delta t / \tau_{pers})$ functions as the correla-

doi:10.6342/NTU202600337

tion factor derived from the relaxation time of an Ornstein-Uhlenbeck process. The term $\sqrt{1-\alpha^2}$ is a scaling factor specifically derived to ensure the process remains stationary with unit variance. This ensures that the perception error maintains a consistent statistical magnitude rather than decaying or diverging over time.

The persistence time τ_{pers}, which dictates the duration of a specific perceptual bias, is implemented as a dynamic parameter to model the *attention shift* phenomenon observed in empirical driving behavior:

- **Opening Up ($\Delta v \leq 0$):** When the gap widens or remains stable, the parameter is maintained at the **default baseline of 10.0 seconds**. This setting represents a nominal cognitive state where perceptual errors tend to persist for longer durations, reflecting the decreased attentional demand on the driver.
- **Closing In ($\Delta v > 0$):** During the phase where the follower approaches the leader, the persistence time τ_{pers} reduces from the baseline to **8.0 seconds**. This shorter relaxation period simulates the heightened alertness of the driver, necessitating more frequent error correction as the perceived risk of collision rises.

3.5.3 Asymmetric Risk Assessment

Unlike machines, human drivers exhibit behavioral hysteresis: they are significantly more conservative when approaching a vehicle than when falling behind. The HCCFM quantifies this psychological safety buffer through a **safety penalty function** Ψ.

The decision-making logic does not use the raw perceived gap g_p. Instead, it calculates an **effective gap** $g_{eff}(t)$, which represents the "mental space" the driver feels is available

doi:10.6342/NTU202600337

$$g_{eff}(t) = \max\{0,\ g_p(t) - \Psi(v_{ego}, \Delta v)\} \tag{3.8}$$

The safety penalty Ψ is formulated to quantify the risk-averse behavior of human drivers, composed of a static buffer and a dynamic kinematic term

$$\Psi = \underbrace{v_f \cdot t_{reac} \cdot C_{static}}_{\text{Base Penalty}} + \underbrace{|\Delta v| \cdot t_{reac} \cdot C_{dynamic}}_{\text{Dynamic Penalty}} \tag{3.9}$$

The *base penalty* is primarily designed to capture the *conservative mindset* of the driver during steady-state cruising. By scaling with the current velocity v_f, it represents a baseline safety margin that drivers maintain to account for inherent uncertainties and to achieve a smooth velocity profile. This term ensures that even in the absence of significant relative speed changes, the system encourages a proactive deceleration that avoids aggressive maneuvers and promotes string stability.

Conversely, the *dynamic penalty* serves as a reactive mechanism that dominates during transient periods of intense acceleration or braking. Since this term is proportional to the absolute velocity difference $|\Delta v|$, its influence remains negligible when the vehicle is cruising at a stable speed relative to the leading vehicle. However, during sudden braking events or rapid closing-in scenarios, the weight of the dynamic penalty escalates rapidly. This shifting dominance allows the model to transition from a "velocity smoothing" mode during stable flow to a "collision avoidance" mode during high-risk maneuvers, effectively capturing the non-linear sensitivity of human drivers to rapid kinematic changes.

Moreover, the coefficient $C_{dynamic}$ is intentionally designed as an asymmetric parameter to capture the behavioral discrepancy between deceleration and acceleration. Empir-

doi:10.6342/NTU202600337

ical observations suggest that human drivers exhibit a heightened sensitivity to potential collisions, leading to urgent braking, while they tend to be more sluggish or hesitant when regaining speed. To mathematically represent this phenomenon, we define $C_{dynamic}$ as follow

$$C_{dynamic} = \begin{cases} C_{decel} \approx 1.5 & \text{if } \Delta v > 0 \text{ (Closing In)} \\ C_{acc} \approx 0.5 & \text{if } \Delta v \leq 0 \text{ (Opening Up)} \end{cases} \tag{3.10}$$

By setting $C_{decel} > C_{acc}$—a relationship further validated through the calibration against empirical data in Section 4.2.1—the safety penalty becomes more sensitive during closing-in scenarios, effectively simulating the tendency of the driver to prioritize safety through immediate and firm braking. Conversely, a lower C_{acc} reflects the observed "slow-to-start" behavior, where the urgency to reduce the safety gap is significantly lower than the urgency to maintain it during braking phases. This asymmetric formulation is crucial for accurately replicating the evolution of traffic shockwaves. As established in the theory of traffic hysteresis [38, 39], the slow recovery of following vehicles relative to their braking response is a primary mechanism driving the persistence and upstream propagation of congestion.

3.5.4 Final Action Determination

Finally, the HCCFM integrates these factors back into the Krauss safety logic. The safe speed v_{safe} is computed by substituting the physical gap $g(t)$ in Eq. 3.2 (Section 3.4) with the psychological effective gap $g_{eff}(t - t_{reac})$, and utilizing the delayed leader velocity

doi:10.6342/NTU202600337

$$v_{safe}^{HCCFM}(t) = V(t - t_{reac}) + \frac{g_{eff}(t - t_{reac}) - V(t - t_{reac})\tau}{\frac{v(t-t_{reac})+V(t-t_{reac})}{2b} + \tau} \tag{3.11}$$

This modified v_{safe} is then used to determine the final actuation command, effectively embedding human cognitive constraints into the vehicle's control loop..

3.6 Speed Advisory System (SAS) Design

Building upon the identified limitations of human cognition in Section 3.5, the SAS is designed as a "Human-in-the-Loop" cooperative controller. Unlike fully autonomous systems that replace the driver, SAS augments human capabilities by converting the driving task from a high-latency, error-prone process into a low-latency, often-deterministic execution task.

3.6.1 Digital State Acquisition and Latency Mitigation

While human drivers rely on delayed visual estimation with a typical physiological reaction time $t_{reac} \approx 1.0$ second, the SAS acquires kinematic data directly via V2X communication. Let $S_{leader}(t) = [x_l(t), v_l(t), a_l(t)]^T$ be the ground truth state of the leading vehicle. The input state available to the SAS controller is

$$S_{SAS}(t) = S_{leader}(t - t_{comm}) \tag{3.12}$$

where t_{comm} represents the network transmission latency. In 5G-V2X environments, t_{comm} is typically less than 50 ms [35]. It is important to note that while t_{comm} is significantly smaller than t_{reac}^{HDV}, the SAS does not entirely eliminate the driver's physical

doi:10.6342/NTU202600337

reaction time. Instead, it effectively removes the **sensing and perception delay**—the time a driver spends estimating the leader's speed and distance visually.

By providing proactive advisories based on this near-real-time state awareness, the SAS allows the driver to begin the physical execution of a maneuver much earlier than if they were relying solely on visual cues. Consequently, the total response time of a CHV is significantly lower than that of an HDV, though it remains constrained by the human's residual movement reaction latency.

3.6.2 Cognitive Load Reduction: From Choice Reaction Time to Simple Reaction Time

The core theoretical contribution of the SAS is the reduction of the effective reaction time. According to Hick's Law [33], unassisted driving is a Choice Reaction Time (CRT) task, where the driver must interpret ambiguous cues and select from multiple possible responses. To quantify this cognitive load, the reaction time (t_{reac}) is modeled logarithmically as a function of the number of available choices (n)

$$t_{reac} = a + b \cdot \log_2(n+1) \tag{3.13}$$

where a represents the simple reaction time processing a known stimulus, and b is a coefficient related to cognitive processing speed.

Consider a typical high-stress braking scenario where the brake lights on the leading vehicle suddenly turned on. The human driver must instantaneously evaluate the situation and choose from at least four potential actions ($n = 4$)

doi:10.6342/NTU202600337

1. **Mild Braking:** Adjust speed slightly to maintain gap.
2. **Emergency Braking:** Decelerate maximally to avoid collision.
3. **Lane Change:** Swerve to an adjacent lane to bypass the obstacle.
4. **No Action:** Decide that the braking is irrelevant and remain unaffected.

Substituting $n = 4$ into Eq. 3.13, the driver incurs a significant penalty due to the selection process ($t_{reac} \propto \log_2(5)$).

In contrast, the SAS simplifies this process by converting the task into a Simple Reaction Time (SRT) paradigm. By presenting a single, calculated directive, e.g., "Accelerate 5 km/h", the system eliminates ambiguity, effectively reducing the choices to a single option ($n = 1$). The theoretical reaction time thus converges towards the minimum

$$t_{reac}^{SAS} \propto \log_2(1+1) = 1 \tag{3.14}$$

Compared to the HDV scenario ($\log_2 5 \approx 2.32$), the SAS theoretically reduces the cognitive processing component by more than half. While the theoretical calculation might suggest an even faster response, to account for residual physical movement delays such as foot movement, and to maintain a safety margin, we conservatively configure the effective reaction time parameter for SAS-equipped vehicles at **0.8 seconds** in our simulation ($t_{reac}^{SAS} = 0.8s$), compared to the human baseline of 1.0 – 1.2 seconds.

3.6.3 Precision-Enabled Stability and Error Elimination

The SAS addresses the instability caused by human perception errors while maintaining a conservative safety profile. The optimization is achieved through two mechanisms:

doi:10.6342/NTU202600337

- **Elimination of Perception Error ($k = 0$):** In the SAS-equipped vehicle, the headway gap is measured via precision sensors such as ToF sensors rather than being visually estimated by the driver. Consequently, the Weber fraction k is set to zero, effectively eliminating the stochastic error term $E(t)$. The perception-level gap available to the system is updated as

$$g_p^{SAS}(t) = g(t - t_{comm}) \tag{3.15}$$

where t_{comm} is the negligible network latency. However, it is important to emphasize that the driver's actual control response is still subject to the **residual movement reaction latency** τ_m. This means that while the information used for decision-making is error-free and near-real-time, the physical execution is based on this state but occurs after the movement delay.

By removing the distance-dependent estimation errors associated with human vision, the SAS eliminates the "phantom" oscillations typically amplified by perceptual uncertainty. The resulting control command is derived from precise kinematic data, allowing the CHV to stabilize the traffic string even while operating within the constraints of human physical response limits.

- **Retention of Asymmetric Safety Logic and Environmental Immunity:** To ensure high safety standards and passenger comfort during manual takeover, the SAS **retains the asymmetric risk coefficients** of the human baseline ($C_{decel} = 1.5, C_{acc} = 0.5$). Unlike the standard Krauss model, which may assume ideal braking conditions, the SAS deliberately preserves the conservative 1.5 multiplier for deceleration gap calculation. This ensures that safety margins remain robust rather than

doi:10.6342/NTU202600337

reducing to the theoretical minimum.

Crucially, the reliance on V2X data grants the system a high degree of **immunity to environmental uncertainties**. While human drivers often increase their safety margins inconsistently or exhibit erratic behavior under varying visibility or complex downstream conditions, the SAS provides stable and deterministic guidance regardless of these external factors. Although the system remains conservative in its risk-taking, the reduced total latency ($t_{reac} = 0.8$ seconds) and minimized headway ($\tau = 0.8$ seconds) allow it to achieve significantly higher road capacity than HDVs. This demonstrates that the efficiency gains stem from **informational determinism and processing speed** rather than aggressive driving maneuvers.

3.6.4 Fail-Safe State Machine and Handover Protocol

To ensure robustness against communication instability such as packet losses, the SAS incorporates a three-state fail-safe logic. The system monitors the "data age", denoted as $\Delta t_{age} = t_{current} - t_{last\_pkt}$, of the V2X signal to determine the operational mode:

1. **Active State ($\Delta t_{age} \leq T_{coast}$):** The system operates normally using fresh V2X data.
2. **Coasting State ($T_{coast} < \Delta t_{age} \leq T_{timeout}$):** If packet loss is intermittent, the system bridges the information gap by predicting the state of the leader using a Constant-Velocity model.
3. **Handover State ($\Delta t_{age} > T_{timeout}$):** If the blackout duration exceeds the critical threshold (set to 1.5 s), the system deems the estimation unreliable and executes an immediate handover to the driver. To prevent hazardous oscillatory control, this

doi:10.6342/NTU202600337

transition is irreversible: the driver permanently disengages the SAS for the remainder of the session.

Compounded Latency and Physiological Realism A critical design consideration is that a human driver cannot instantly assume control with perfect situational awareness immediately after a system dropout. To capture this vulnerability, we model the transition process using a **compounded latency** mechanism. This metric represents the realistic total time delay before effective human braking occurs, calculated as the sum of the system timeout threshold and the inherent reaction time of the driver:

$$T_{total\_delay} = T_{timeout} + t_{reac}^{HDV} = 1.5s + 1.0s = 2.5s \tag{3.16}$$

This 2.5-second handover sequence unfolds in three distinct phases, integrating the system logic with the cognitive recovery of the driver:

1. **Phase 1: System Holding (**$0s \rightarrow 1.5s$**):** Corresponds to the *coasting state*. Upon packet loss, the system attempts to bridge the gap using the constant velocity estimator. During this 1.5-second interval, the human driver remains passive, relying on the system to handle the control logic.

2. **Phase 2: Cognitive Processing & Penalty (**$1.5s \rightarrow 2.5s$**):** At time $t = 1.5\,\text{s}$, the system declares a failure and issues a take-over request. Crucially, the control logic enforces a *re-acquisition penalty*: the reaction time of the driver resets to the human baseline ($t_{reac}^{HDV} \approx 1.0\,\text{s}$), and the input state reverts to visual perception. This interval simulates the time required for the driver to visually re-acquire the traffic context and physically move the foot to the brake pedal.

doi:10.6342/NTU202600337

3. **Phase 3: Action Execution ($t > 2.5s$):** The driver successfully regains control. At this timestamp, 2.5 seconds post-disconnection, the manual takeover is complete; the SAS is deactivated, and the vehicle effectively reverts to the HDV operational state.

doi:10.6342/NTU202600337

Chapter 4

Implementation

This chapter details the experimental implementation framework used to validate the proposed system. We first introduce the simulation environment architecture based on SUMO and TraCI. Subsequently, we describe the rigorous calibration process of the HC-CFM using an empirical dataset to ensure behavioral realism. Finally, we define the specific experimental scenarios—including microscopic pulse tests, macroscopic bottlenecks, and network reliability tests—designed to comprehensively evaluate the performance of the system.

4.1 Simulation Environment

An overview of the system architecture is illustrated in Figure 4.1. The SUMO simulator is controlled through the Traffic Control Interface (TraCI) to set vehicle variables during the simulation using Python scripts.

The system architecture follows a closed-loop control strategy where the vehicle states are retrieved, processed by the proposed driver model, and updated in real-time.

doi:10.6342/NTU202600337

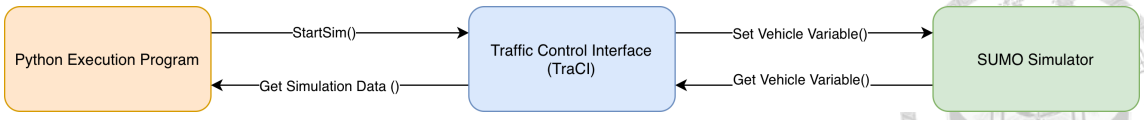

Figure 4.1: Traffic Manager Control Logic using Python.

The simulation step length is configured to a high-resolution setting of **0.1 seconds**. Consequently, it is important to note that the vehicle data retrieved via TraCI at the current step t corresponds to the simulation state at $(t - 0.1)$ second, the immediate preceding step. This discrete time-stepping mechanism ensures causal consistency, where the control logic computes the actuation for the current step based on the observed state from the previous step.

4.2 Vehicle Model Implementation and Calibration

This section details the implementation of the Human-Driven Vehicle (HDV) and the SAS-equipped vehicle models. To ensure the simulation reflects realistic traffic dynamics, we conducted a rigorous two-phase calibration process: a microscopic calibration to replicate individual car-following behaviors, and a macroscopic calibration to reproduce aggregate flow characteristics and capacity drops in bottleneck scenarios.

4.2.1 Calibration Methodology

The calibration process aims to determine the parameter set that maximizes the fidelity of the HCCFM, ensuring the model faithfully reproduces real-world driving behaviors. To capture both realistic human driving dynamics and local traffic characteristics, we conducted a rigorous **two-phase calibration process** utilizing distinct datasets for different scales. Phase 1 focuses on microscopic behavioral realism using the **NGSIM US-101**

doi:10.6342/NTU202600337

dataset, while Phase 2 targets macroscopic capacity constraints using local data from **Taiwan's National Freeway No. 5**.

Rationale for Hybrid Dataset Selection

To overcome data availability limitations while ensuring both behavioral fidelity and local relevance, this hybrid calibration strategy was adopted. The **NGSIM US-101 dataset** [40] was selected for microscopic calibration due to its provision of high-resolution vehicle trajectories (x, y, v, a), which are absent in the aggregated macroscopic metrics provided by Taiwan's Traffic Detection Control System (TDCS). Complementarily, macroscopic parameters were calibrated using local data from **Taiwan's National Freeway No. 5** [41] to accurately capture specific environmental constraints and reproduce the realistic capacity drop observed in the tunnel environment.

Phase 1: Microscopic Calibration

To capture the nuances of human driving, we utilized real-world trajectory data from the **NGSIM US-101 dataset** [40]. The calibration focused on determining the three novel conservative coefficients in Eqs. 3.9 and 3.10—C_{static}, C_{decel}, and C_{acc}—under the assumption that the average human driver possesses a reaction time (t_{reac}) and minimum time headway (τ) of approximately 1.0 second. The process was divided into two stages:

1. **Stage 1: Static Coefficient (C_{static}):** We extracted "steady-state" consecutive leader-follower trajectory pairs where the relative velocity was near zero ($\Delta v \approx 0$). In these stable conditions, the dynamic penalty terms vanish, allowing us to isolate and calibrate the baseline risk perception (C_{static}) to match the observed following

doi:10.6342/NTU202600337

distances.

2. **Stage 2: Dynamic Coefficients (C_{decel}, C_{acc}):** Using volatile "stop-and-go" traffic data, we calibrated the dynamic responses to relative speed:

   - C_{decel}, which governs the safety margin during deceleration as defined in Eq. 3.10, was tuned during "closing-in" phases ($\Delta v > 0$) to capture the heightened caution and braking magnitude when approaching a slower leader, yielding a converged value of approximately **1.5**.
   - C_{acc}, the acceleration sensitivity coefficient introduced in Eq. 3.10, was tuned during "opening-up" phases ($\Delta v \leq 0$) to reflect the characteristic lag or hesitation in acceleration when the leader pulls away, resulting in a coefficient of **0.5**.

Phase 2: Macroscopic Calibration

To ensure the *virtual bottleneck* scenario (defined in Section 4.3) accurately reflects real-world traffic breakdown, we performed a macroscopic calibration using empirical data from the **National Freeway No. 5 in Taiwan**.

We analyzed data from the Traffic Detection Control System (TDCS) [41], specifically comparing the maximum throughput of an open road section (Gantry 05F0055N) against a tunnel bottleneck section (Gantry 05F0287N) during peak hours. The empirical data revealed a physical **capacity drop of approximately 12.6%** within the tunnel environment.

To accurately reflect this phenomenon, a **reverse-calibration process** was applied to the behavioral parameters of the simulation. The HDV settings within the bottleneck zone

doi:10.6342/NTU202600337

were iteratively adjusted, specifically by increasing the reaction time t_{reac} to 1.2 seconds and the deceleration coefficient C_{decel} to 1.8. These specific values were established precisely because they yield a simulated capacity reduction that converges with the empirical 12.6% degradation, thereby ensuring the numerical fidelity of the bottleneck model.

4.2.2 Parameter Configuration

Based on the calibration methodology described above, the final parameter configurations for both HDV and SAS vehicles were established. To accurately model varying traffic environments, these configurations are categorized into "open road" and "bottleneck" modes. The latter specifically corresponds to the high-stress conditions within the virtual bottleneck scenario detailed in Section 4.3.2, ensuring the model reflects the capacity degradation observed in empirical tunnel data. Table 4.1 summarizes the calibrated values used throughout the experiments. These parameters are not merely numerical inputs but represent specific behavioral characteristics of human drivers and the SAS controller under varying traffic conditions. The following insights highlight the rationale behind these configurations and their implications for traffic stability:

- **Bottleneck-Induced Stress (HDV):** Within the bottleneck zone, the HDV parameters are calibrated to represent a high-stress state. The increased reaction time of 1.2 seconds and the heightened deceleration coefficient of 1.8 model the cognitive load and excessive caution that typically lead to capacity drops in confined environments such as tunnels.

- **Standard SAS Optimization (Open Road):** In standard open-road conditions, the SAS prioritizes maximum efficiency. It operates with a reduced reaction time of

doi:10.6342/NTU202600337

Table 4.1: Calibrated Model Parameters for HDV and SAS

Parameter	**Sym.**	**HDV** *(Open)*	**HDV** *(Bottle.)*	**SAS** *(Open)*	**SAS** *(Bottle.)*	**Description**
Reaction Time	t_{reac}	1.0 s	1.2 s	0.8 s	1.0 s	Delay between Perception and Action
Min Headway	τ	1.0 s	1.2 s	0.8 s	1.0 s	Desired minimum time gap
Weber Fraction	k	0.1	0.1	**0.0**	**0.0**	Spatial perception error rate (Noise)
Static Coeff	C_{static}	0.5	0.5	0.5	0.5	Baseline safety buffer
Decel Coeff	C_{decel}	1.5	**1.8**	1.5	1.5	Risk aversion (Closing gaps)
Accel Coeff	C_{acc}	0.5	**0.75**	0.5	0.5	Recovery lag (Opening gaps)

0.8 seconds and eliminates perception error ($k = 0$), optimizing traffic flow while maintaining safe mechanical limits.

- **Bottleneck Configuration (SAS-Bottle):** Within bottleneck zones, the SAS **exclusively adopts** a "Ready-to-Handover" profile. Instead of maximizing efficiency with tight 0.8-second gaps, the system maintains a relaxed headway parameter of 1.0 second throughout the bottleneck segment. This strategic buffer prevents the formation of extreme gaps that would be physiologically unmanageable for a driver to inherit, thereby ensuring that the vehicle state remains constantly primed for a safe manual transition should disengagement occur in these critical zones.

4.2.3 Baseline Models Configuration

To rigorously validate the proposed HCCFM, we employ two distinct baseline models for comparative analysis, representing different levels of behavioral fidelity:

1. **Standard Krauss Model (Baseline 1):** As the default car-following model in SUMO, Krauss represents the standard "Collision-Free" logic. It assumes imperfect driving

doi:10.6342/NTU202600337

mainly through a stochastic *sigma* parameter, lacking temporal error persistence.

2. **Extended Intelligent Driver Model (EIDM) (Baseline 2):** Representing the state-of-the-art in modeling smooth, human-like, and jerk-limited driving dynamics. For a fair comparison, we configured the EIDM with a reaction time of 0.8 seconds and calibrated the *tPersEstimate* parameter to match the error persistence observed in the NGSIM dataset.

4.2.4 Evaluation Metrics

Beyond the scalar Root Mean Square Error (RMSE), we introduce probabilistic metrics to evaluate the distributional fidelity of the models:

- **Cumulative Distribution Function (CDF) of Error:** Used to assess the proportion of simulation steps where the velocity error falls within specific bounds.
- **Kernel Density Estimation (KDE):** Used to visualize the probability density function of errors, allowing us to inspect the bias and kurtosis of the model performance relative to human trajectories.

4.3 Experimental Scenarios

Two distinct scenarios were designed to evaluate the system from microscopic and macroscopic perspectives.

4.3.1 Pulse Step Test Scenario

This scenario evaluates the system ability to mitigate shockwave propagation. A leading vehicle, labelled as “vehicle 0”, is trajectory-controlled to execute a specific per-

doi:10.6342/NTU202600337

turbation profile, as shown in Figure 4.2, while a platoon of 300 followers reacts to this disturbance.

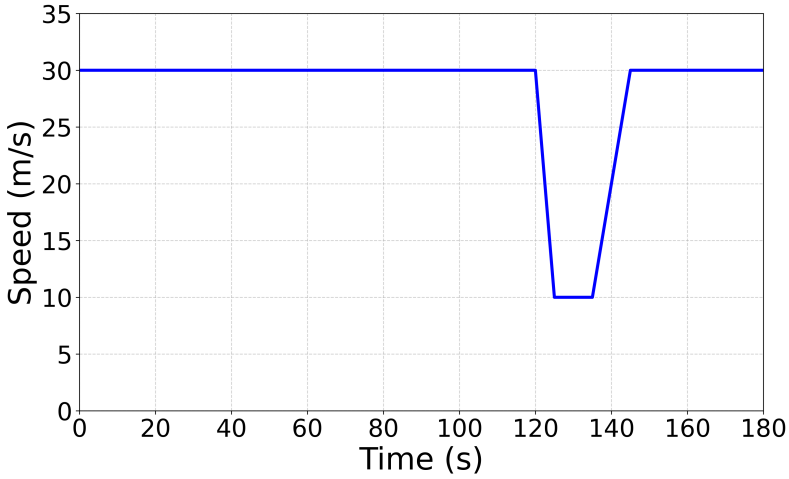

Figure 4.2: Leading vehicle speed through out the simulation.

- **0-120s:** Constant speed cruising at 30 m/s to stabilize the platoon.
- **120-125s:** Rapid deceleration at 4 m/s^2 to 10 m/s, simulating a hard braking event similar to reacting to a cut-in.
- **125s-135s:** Holding speed at 10 m/s for 10 seconds.
- **135s-145s:** Recovery acceleration at 2 m/s^2 back to 30 m/s.

This severe "stop-and-go" event allows for the measurement of shockwave propagation length, recovery time and string stability.

4.3.2 Virtual Bottleneck Scenario

To measure the maximum road capacity, a *virtual bottleneck* is implemented to force a traffic breakdown. Unlike a lane reduction, this method creates a localized zone of reduced efficiency. The defined zone represents an area with reduced visibility or geometric

doi:10.6342/NTU202600337

constraints such as a tunnel or curve. For HDVs, this environmental stress forces an increase in reaction time ($t_{reac} : 1.0s \rightarrow 1.2s$) and time headway ($\tau : 1.0s \rightarrow 1.2s$). Furthermore, the conservative coefficients are heightened ($C_{decel} : 1.5 \rightarrow 1.8$; $C_{acc} : 0.5 \rightarrow 0.75$), simulating the natural human tendency to drive cautiously and sluggishly in restricted environments.

In contrast, while the SAS-equipped vehicles are assumed to rely on onboard sensors such as radar or LiDAR, which are *immune to environmental constraints* including low lighting or geometric restrictions, a safety-oriented adjustment is implemented within the bottleneck zone. **To facilitate a safe potential handover to human control**, the system proactively relaxes its aggressive following parameters.

Specifically, both reaction time and headway are adjusted to **1.0 second** inside the zone. While this is less aggressive than the 0.8-second-open-road SAS setting, it avoids the critical instability that might occur if a human driver were suddenly forced to take over at an extreme close range. This strategy serves as a *ready-to-handover* state, balancing operational efficiency with fail-safe readiness.

To accurately measure the macroscopic road capacity, a standard point-based induction loop detector—implemented as an E1 detector in SUMO—is installed at the location x=3510m, immediately downstream of the bottleneck zone (3000m−3500m), as shown in Figure 4.3. This specific placement is critical for capturing the queue discharge flow—the maximum stabilized flow rate as vehicles accelerate out of the congested area. The detector is configured to aggregate traffic flow and density data at 60-second intervals. This temporal resolution is sufficient to construct the Fundamental Diagram while effectively smoothing out microscopic fluctuations caused by individual vehicle interactions.

doi:10.6342/NTU202600337

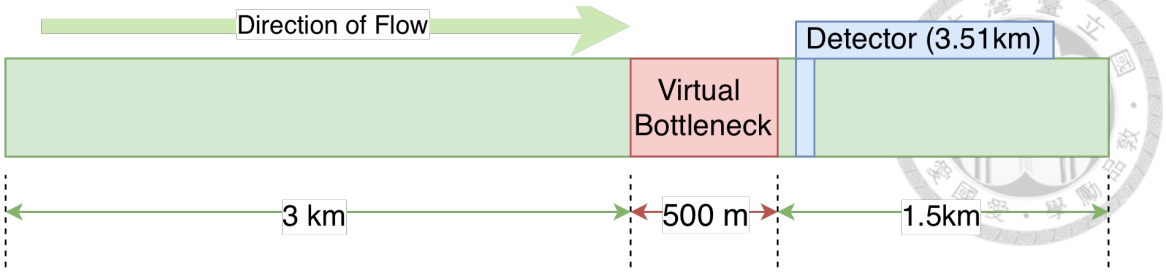

Figure 4.3: Virtual bottleneck set up.

4.3.3 Penetration Rate Sensitivity

In real-world deployment, the transition to fully automated or assisted driving will be gradual. To evaluate the robustness of the proposed system during this transition, we conducted a sensitivity analysis regarding the market penetration rate. This analysis investigates the impact of the system from two distinct perspectives:

1. **Macroscopic Capacity:** Evaluating how the maximum sustainable flow rate of the bottleneck improves as the proportion of SAS vehicles increases from 0% to 100%.

2. **Microscopic Stability:** Evaluating the mitigation of shockwaves propagation distance and the reduction of congestion time under the *pulse step* perturbation scenario.

The vehicle stream is modeled as a mixed traffic environment. The penetration rate (PR) is defined as follow

$$PR = \frac{N_{SAS}}{N_{HDV} + N_{SAS}} \times 100\% \tag{4.1}$$

where N_{HDV} denotes the total number of HDVs not equipped with SAS, and N_{SAS} the total number of SAS-equipped vehicles. Simulations are executed at penetration levels

doi:10.6342/NTU202600337

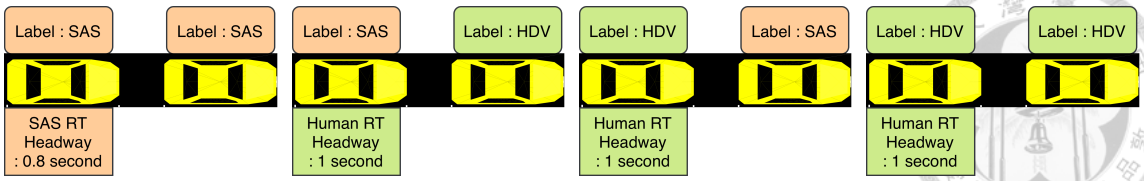

(a) Case 1: SAS-SAS (Active) (b) Case 2: SAS-HDV (Fallback) (c) Case 3: HDV-SAS (d) Case 4: HDV-HDV

Figure 4.4: Interaction scenarios and parameter settings for different lead-following vehicle pairs. The optimized SAS parameter set is activated only in Case 1.

ranging between 0% and 100% with increments of 10%.

Interaction Logic and Degradation Mechanism

While the penetration rate defines the overall proportion of equipped vehicles, the activation of the advanced control features is governed by a strict pair-wise interaction logic. Unlike standalone systems, the proposed SAS is designed to optimize flow cooperatively.

Consequently, the SAS operational mode, characterized by a reduced headway and machine reaction time of 0.8 seconds, is triggered **if and only if** the following vehicle is SAS-equipped **and** the leading vehicle is also SAS-equipped. This dependency ensures that the tighter following gap is supported by the predictability or communication capability of the leading vehicle.

In all other scenarios—specifically when an SAS vehicle follows a HDV—the system degrades to a conservative mode. In this fallback state, the SAS vehicle adopts the behavioral parameters of a standard HDV with 1.0 second headway and human reaction time to maintain safety margins against the stochastic behavior of the unequipped leader.

The specific interaction behaviors for all four possible car-following pairs are presented in Figure 4.4.

Let M_n be the active controller mode of vehicle n. The control logic is formally

doi:10.6342/NTU202600337

determined by

$$M_n = \begin{cases} \text{SAS}, & \text{if } Type(n) = \text{SAS} \wedge Type(n-1) = \text{SAS} \\ \text{HDV}, & \text{otherwise} \end{cases} \tag{4.2}$$

where $Type(n)$ denotes the equipment class of the subject vehicle, and $Type(n-1)$ denotes that of the leading vehicle.

4.3.4 Network Reliability and Fail-Safe Mechanism

To assess the robustness of the syste against realistic communication failures, a **Gilbert-Elliot Model** is implemented to simulate 5G packet loss. Unlike simple stochastic models, this approach captures the "bursty" nature of channel fading, where packet losses tend to occur in consecutive clusters.

1. Gilbert-Elliot Channel Model

The communication link is modeled as a two-state Markov chain comprising a **Good State (G)** and a **Bad State (B)**.

- **Good State (G):** Packet delivery is successful.
- **Bad State (B):** Packet is lost.

Let p be the transition probability from Good to Bad ($G \to B$), and r be the transition probability from Bad to Good ($B \to G$). These probabilities are derived from two configurable parameters: the **packet loss rate (P_{loss})** and the **average burst length (L_{burst})**.

doi:10.6342/NTU202600337

The probability r is the inverse of the average burst length, representing the likelihood of recovering from a fade

$$r = \frac{1}{L_{burst}} \tag{4.3}$$

The probability p is then determined to satisfy the steady-state packet loss rate P_{loss}

$$p = \frac{P_{loss} \cdot r}{1 - P_{loss}} \tag{4.4}$$

In this study, simulations are conducted under varying P_{loss} conditions while maintaining a fixed burst length of 1.5 seconds.

2. State Estimation Strategy

During communication blackouts, the ego vehicle loses access to the real-time kinematics of the leader. To bridge these gaps and maintain control continuity, this study adopts a **Constant Velocity (CV)** assumption. This strategy begins by calculating the elapsed time since the last successful V2X transmission

$$\Delta t = t - t_{last} \tag{4.5}$$

where t_{last} is the timestamp of the last received packet. To ensure a conservative estimation that prioritizes string stability over aggressive tracking, we assume that the leader maintains its speed without further acceleration during the blackout period

$$\hat{a}_{lead}(t) = 0 \tag{4.6}$$

doi:10.6342/NTU202600337

Consequently, the estimated velocity of the leading vehicle ($\hat{v}_{lead}$) is held constant, set to the value recorded at the final successful communication event

$$\hat{v}_{lead}(t) = v_{lead}(t_{last}) \tag{4.7}$$

Finally, the estimated gap ($\hat{g}$) at the current time t is projected by integrating the relative velocity difference over the blackout duration Δt

$$\hat{g}(t) = g(t_{last}) + (v_{lead}(t_{last}) - v_{ego}(t)) \cdot \Delta t \tag{4.8}$$

This approach ensures that the SAS controller operates on deterministic, albeit slightly outdated, kinematic logic. By assuming constant velocity, the system prevents erratic maneuvers or sudden speed spikes that could be triggered by erroneous or noisy estimation of the leader's higher-order dynamics during the period of uncertainty.

3. Fail-Safe Degradation Mechanism

To ensure safety during prolonged disconnects, a strict timeout threshold is enforced. If the communication blackout persists for more than **1.5 seconds** ($\Delta t > 1.5s$), the system deems the estimation unreliable and triggers a **fail-safe mode**.

In this mode, control authority is reverted to the HDV logic. Specifically, to simulate the cognitive limits of a human driver suddenly re-engaging with the task, the fallback inputs are subject to human reaction latency ($t_{reac}^{HDV} \approx 1.0s$).

doi:10.6342/NTU202600337

$$Mode(t) = \begin{cases} \text{SAS (Estimated)}, & \text{if } \Delta t \leq 1.5s \\ \text{HDV (Fallback)}, & \text{if } \Delta t > 1.5s \end{cases} \tag{4.9}$$

For the HDV fallback, the effective perception utilizes data from the reaction period. This implies that when the driver takes control at $\Delta t = 2.5$ s, they are reacting to the traffic state observed 1.0 second prior, which is at $t = 1.5$ seconds. This results in a compounded latency effect that ensures a realistic worst-case safety assessment.

4.3.5 Two-Lane Capacity Scenario with Lane Changing Dynamics

The scenarios described previously focused exclusively on longitudinal vehicle dynamics within a single-lane environment. However, real-world highway capacity is heavily influenced by lateral interactions, specifically lane-changing maneuvers, which often serve as significant sources of perturbation. To address this limitation and evaluate the system applicability in realistic traffic, a *two-lane highway* scenario is introduced.

In this setup, the simulation environment is expanded to a dual-lane configuration where vehicles are permitted to execute lane changes. The lateral behavior is governed by the default lane-changing model in SUMO, which dictates maneuvers based on strategic routing, cooperative adjustments, and tactical speed gains.

Lane-Changing Incentive: Speed Heterogeneity

To induce realistic overtaking maneuvers and justify the need for lane changing, a strict homogeneity of vehicle speeds must be broken. If all vehicles travelled at identical desired speeds, no driver would have the incentive to change lanes for speed gain.

doi:10.6342/NTU202600337

Therefore, *speed heterogeneity* is introduced into the traffic stream. Instead of a fixed velocity, the desired speed of each vehicle is sampled from a normal distribution with a mean of 30 m/s and a standard deviation of 3 m/s. This variance creates natural speed differentials between followers and leaders, providing the necessary incentive for faster vehicles to seek overtaking opportunities. This setup introduces two critical perturbation sources:

- **Overtaking Demand:** Faster vehicles aggressively seeking gaps to bypass slower traffic.
- **Cut-in Disturbances:** Vehicles entering a lane force followers to adjust their spacing, potentially triggering shockwaves.

Similar to the single-lane benchmark, the primary objective of this scenario is to determine the maximum achievable capacity of the two-lane cross-section under varying SAS penetration rate from 0% to 100%. This test investigates whether the longitudinal stability benefits provided by SAS can effectively translate into capacity gains even in the presence of lateral disruptions caused by this speed heterogeneity.

doi:10.6342/NTU202600337

Chapter 5

Evaluation

5.1 Overview

This chapter presents a comprehensive evaluation of the proposed SAS. The primary objective is to quantify the effectiveness of the system in mitigating traffic shockwaves and improving overall road capacity within a mixed autonomy environment. To ensure a rigorous assessment, the evaluation is organized into six logical phases, progressing from microscopic verification to macroscopic performance and robustness analysis:

1. **Model Calibration and Validation (Section 5.2):** First, the HCCFM is calibrated against the NGSIM dataset to establish a realistic behavioral baseline, ensuring that the simulation accurately reflects human reaction latencies and hesitation.

2. **Microscopic String Stability (Section 5.3):** We utilize the *pulse step* stress test to validate the mechanism of action. This section analyzes how the reduced reaction time actively dampens shockwave propagation and minimizes total delay at the individual platoon level.

doi:10.6342/NTU202600337

3. **Macroscopic Capacity Analysis (Section 5.4):** Building upon microscopic stability, the study expands to the *virtual bottleneck* scenario. We analyze the Fundamental Diagram to quantify the concrete percentage improvement in capacity achieved by the SAS.

4. **Sensitivity Analysis: Penetration Rate (Section 5.5):** To assess feasibility during the transitional period, this section evaluates performance across varying market penetration rate. It investigates the *critical mass* effect required to observe significant reductions in traffic delay.

5. **Impact of Network Reliability (Section 5.6):** Recognizing the reality of communication instability, we evaluate the robustness of the system using a Gilbert-Elliot packet loss model. This section verifies the effectiveness of the proposed fail-safe mechanism in preventing collisions during data blackouts.

6. **Two-Lane Capacity Analysis (Section 5.7):** Finally, the evaluation extends to a realistic multi-lane highway environment with frequent lane-changing maneuvers. This section tests whether the longitudinal stability benefits of SAS can effectively translate into capacity gains in the presence of lateral disturbances.

5.2 Model Calibration and Validation

Before evaluating the macroscopic road capacity, it is essential to verify the fundamental mechanism of the proposed system. This section presents the validation of the HCCFM against the NGSIM dataset, benchmarking it against both baselines, the standard Krauss model and the EIDM, respectively.

doi:10.6342/NTU202600337

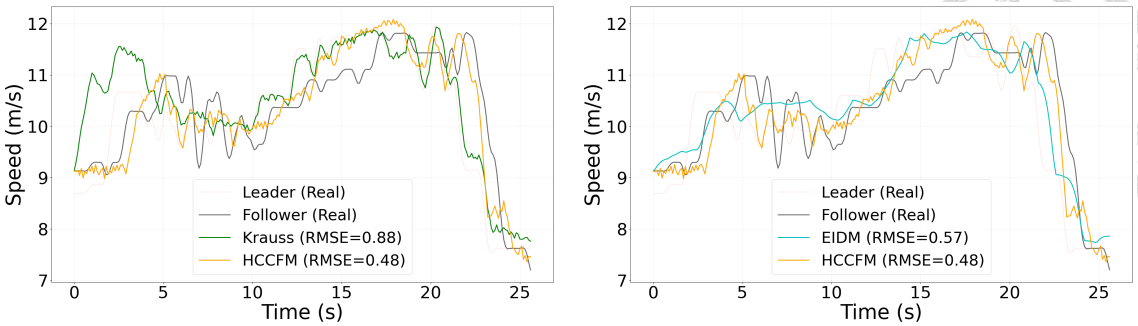

(a) Comparison with Standard Krauss Model (b) Comparison with EIDM Baseline

Figure 5.1: Velocity profile comparison for NGSIM Pair 707-704. (a) The Krauss model (Green) exhibits excessive high-frequency jitter. (b) The EIDM (Cyan) is overly smooth and robotic. The HCCFM (Orange) best captures the human-like drift and correction cycles.

5.2.1 Trajectory Reproduction Capability

We first analyze the velocity profiles for the highly dynamic NGSIM consecutive vehicle pair 707-704 to evaluate how well each model replicates human fluctuations.

- **Krauss (Figure 5.1a): Unrealistic tight coupling.** The standard Krauss model exhibits "super-human" responsiveness due to its reaction time being coupled with the simulation step set to 0.1 seconds. This near-perfect reaction capability causes the vehicle to track the velocity of the leader profile too closely, resulting in a trajectory that "sticks" to the leader and deviates significantly from the lagged, looser following behavior observed in real human driving, leading to the highest RMSE of 0.88 m/s.

- **EIDM (Figure 5.1b): Overly smooth profile.** In contrast, the EIDM generates a trajectory that is mathematically ideal but *excessively smooth*. While it mitigates the tracking error, its jerk-minimizing logic results in a robotic profile that fails to capture the stochastic "drift and correction" micro-behaviors inherent in human driving, making it distinguishable from the ground truth data. However, incorporating the

doi:10.6342/NTU202600337

reaction time concept successfully leads to a lower RMSE of 0.57 m/s.

- **HCCFM Performance:** The HCCFM achieves the best alignment with the ground truth. Its superior performance stems from explicitly modeling **physiological reaction latency** and **asymmetric risk perception**. These mechanisms allow the model to accurately replicate the natural delays and "firm braking, gradual recovery" dynamics of human drivers, resulting in the lowest RMSE of $0.47\ m/s$.

To ensure robustness, we evaluated the models across 23 distinct trajectory pairs. The results showed that the HCCFM consistently outperforms both baselines, achieveing a lower mean RMSE of 1.10 m/s compared to Krauss and EIDM, which are 1.18 m/s and 1.48 m/s respectively, indicating that the proposed model adapts better to the noisy reality of the NGSIM dataset.

5.2.2 Probabilistic Error Analysis (KDE & CDF)

Beyond scalar metrics like RMSE, we analyze the distributional characteristics of velocity errors to assess the behavioral fidelity of the model. Figure 5.2 and Figure 5.3 present the Kernel Density Estimation (KDE) and Cumulative Distribution Function (CDF) of the error, respectively.

The KDE analysis, as shown in Figure 5.2, reveals that the HCCFM exhibits a highly **leptokurtic** error distribution compared to the flatter, wider distributions of both the Krauss and EIDM baselines. The probability density peaks sharply around zero, indicating that for the vast majority of simulation steps, the HCCFM maintains a high degree of precision with minimal deviation from the ground truth.

This observation is quantitatively corroborated by the CDF analysis as shown in Fig-

doi:10.6342/NTU202600337

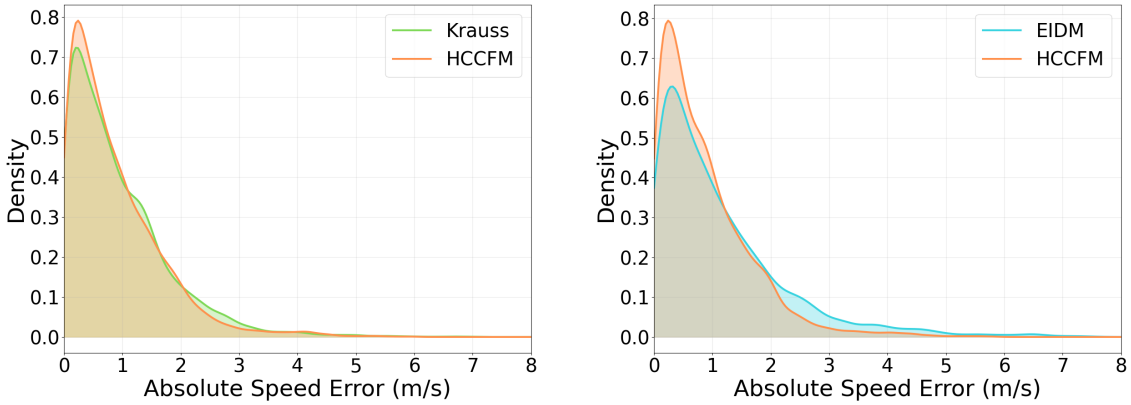

(a) KDE: HCCFM vs Krauss

(b) KDE: HCCFM vs EIDM

Figure 5.2: Kernel Density Estimation (KDE) of velocity errors. The HCCFM (Orange) exhibits a higher peak density around zero (leptokurtic distribution) compared to both baselines, indicating higher precision and stability.

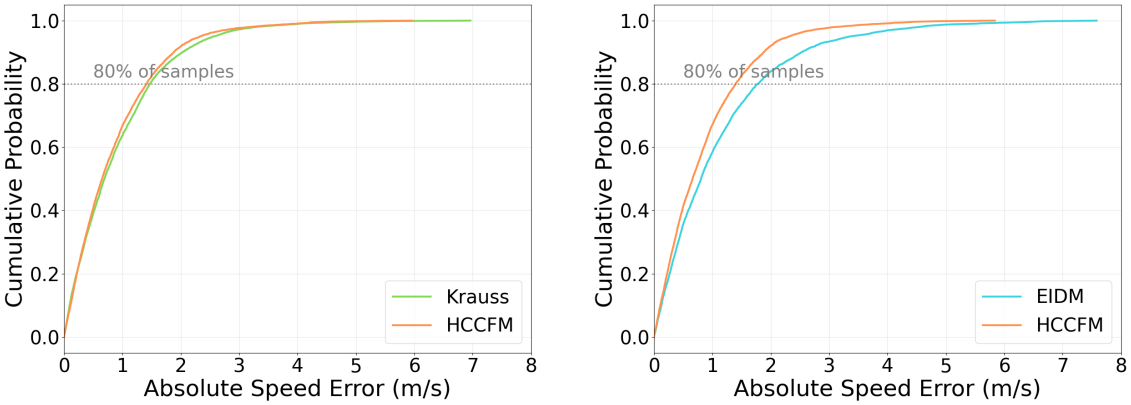

(a) CDF: HCCFM vs Krauss

(b) CDF: HCCFM vs EIDM

Figure 5.3: Cumulative Distribution Function (CDF) comparison. The HCCFM curve (Orange) rises slightly steeper than both baselines, indicating a higher probability of maintaining low error margins.

doi:10.6342/NTU202600337

ure 5.3. The HCCFM curve rises slightly steeper than the baselines, demonstrating superior error containment. Specifically, the probability of the absolute error remaining below $1.0\ m/s$ is consistently higher for our proposed model. This confirms that by integrating the distance-dependent Weber-Wiener process and the reaction time mechanism, the HCCFM effectively mitigates the large, stochastic deviations often observed in standard models, resulting in a more reliable and human-like behavioral prediction.

5.3 Microscopic String Stability of SAS

To rigorously evaluate the stabilizing effect of the SAS, we conducted the *pulse step* stress test. In this scenario, the leading vehicle executes a sharp deceleration from $30\ m/s$ to $10\ m/s$ followed by an acceleration, creating a severe perturbation. The stability performance is analyzed from three complementary perspectives:

1. **Qualitative Visual Analysis:** Using Space-time heatmaps to visualize shockwave dissipation.
2. **Quantitative Impact:** Measuring shockwave propagation distance and total delay time.
3. **Mechanism Verification:** Analyzing the amplification ratio to prove the physical attenuation of the disturbance energy.

5.3.1 Qualitative Analysis: Space-Time Heatmaps

To intuitively visualize the propagation of the traffic shockwave, we employed space-time heatmaps, where the color intensity represents the local speed of vehicles. Figure 5.4

doi:10.6342/NTU202600337

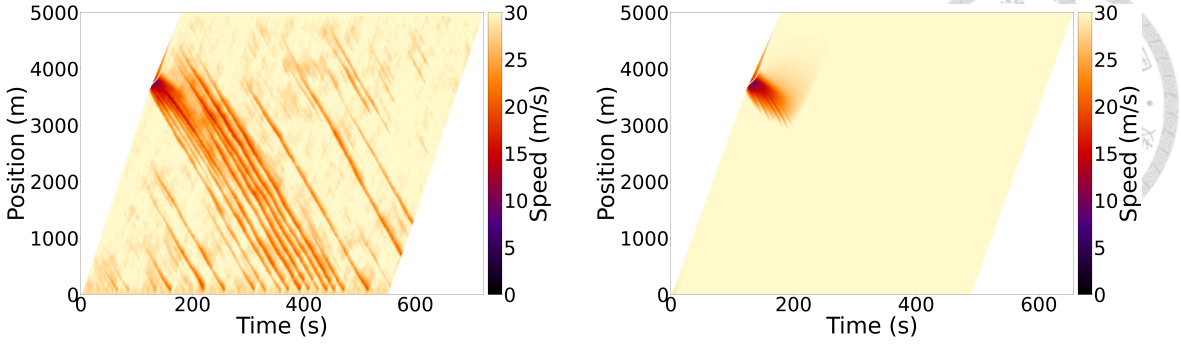

(a) HDV Baseline

(b) SAS Integrated

Figure 5.4: Space-time heatmaps comparing shockwave propagation. (a) HDV Baseline: The dark red band (indicating low speed $15m/s$) propagates to the end of the car flow. (b) SAS Integrated: The shockwave is visibly truncated. The red congestion wave transitions to lighter colors (yellow/white) instantaneously, indicating a quick recovery to free-flow speed.

contrasts the traffic flow evolution between the HDV baseline and the SAS-integrated platoon. The detailed observation of the two figures are furthered discussed as follow:

- **HDV Baseline (Figure 5.4a): Unbounded propagation.** In the pure HDV scenario, the shockwave exhibits a clear *amplification* characteristic. The **deep red band** indicating severe congestion with speed $< 15m/s$ does not dissipate; instead, it propagates continuously upstream from the leader to the very tail of the platoon. This indicates that the disturbance is preserved and even intensified as it travels, forcing every subsequent driver to go through a stop-and-go scenario.

- **SAS Integrated (Figure 5.4b): Rapid convergence.** In strong contrast, the SAS scenario demonstrates an *over-damped* characteristic. The shockwave is visibly **truncated**. The deep red congestion zone is confined to only the first few vehicles and vanishes rapidly within a short spatial range. The wave fails to propagate downstream, transitioning quickly into lighter yellow and white colors, which signifies a quick recovery to free-flow speed.

doi:10.6342/NTU202600337

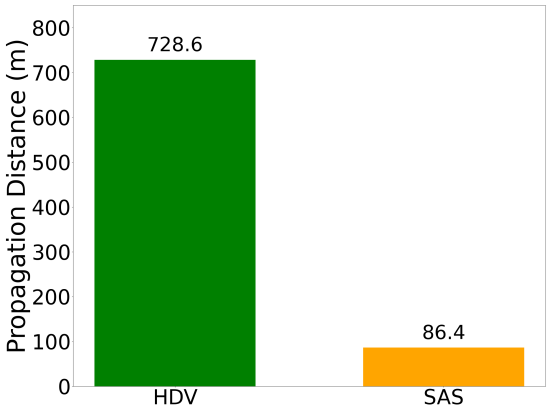

(a) Propagation distance difference.

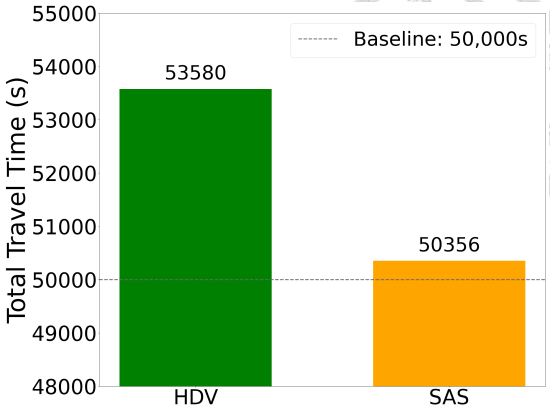

(b) Total delay time difference.

Figure 5.5: Quantitative stability metrics. (a) The shockwave propagation distance drops significantly with SAS adoption. (b) Total delay time exhibits a dramatic decrease.

This visual comparison confirms that the SAS acts as a **low-pass filter** for traffic disturbances, effectively filtering out high-frequency stop-and-go oscillations before they can propagate through the platoon.

5.3.2 Quantitative Impact: Propagation Distance and Delay

We further quantified the effectiveness of the system using two key metrics: **propagation distance** and **total delay time**. It is important to note that the results presented in this section are derived from a single representative simulation instance of the pulse step scenario, rather than a statistical average. This specific selection allows for a clear isolation of the kinematic evolution of the shockwave under a deterministic perturbation.

1. Propagation Distance: As shown in Figure 5.5a, the shockwave in the pure HDV environment propagated approximately **728.6 meters** upstream. With the introduction of SAS, this distance decreases significantly, limiting to only **86.4 meters**, representing a reduction of **88%**. This confirms that SAS vehicles act as effective "wave breakers," spatially confining the congestion.

doi:10.6342/NTU202600337

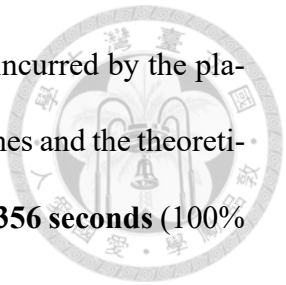

2. Total Delay Time: Figure 5.5b illustrates the total time loss incurred by the platoon, defined as the cumulative difference between the actual travel times and the theoretical free-flow baseline. The delay drops from **3580 seconds** (HDV) to **356 seconds** (100% SAS), representing a massive **90% improvement**.

5.3.3 Mechanism Verification: Perturbation Amplification Ratio

While the previous metrics demonstrate that the system works, this section analyzes how it works by examining the **perturbation amplification ratio**. This metric is defined as the ratio of the maximum velocity drop of the n-th vehicle (Δv_n) to that of the leader (Δv_{leader})

$$\text{Ratio}_n = \frac{v_{free\_flow} - v_{min,n}}{\Delta v_{leader}} \tag{5.1}$$

A ratio > 1.0 indicates instability and shockwave amplification, while a ratio < 1.0 indicates stability and damping effect.

Figure 5.6 reveals the fundamental difference in control physics between human drivers and the SAS:

- **HDV Baseline (Green Line):** The human driver platoon exhibits **marginal stability**. The ratio fluctuates between 0.6 and 1.0 but fails to decay significantly even after 100 vehicles. This "stagnant convergence" explains the persistence of phantom traffic jams on real highways; while the disturbance remains bounded, it exhibits negligible attenuation, resulting in sustained downstream oscillations.
- **SAS (Orange Line):** The proposed system demonstrates **strong damping**. The

doi:10.6342/NTU202600337

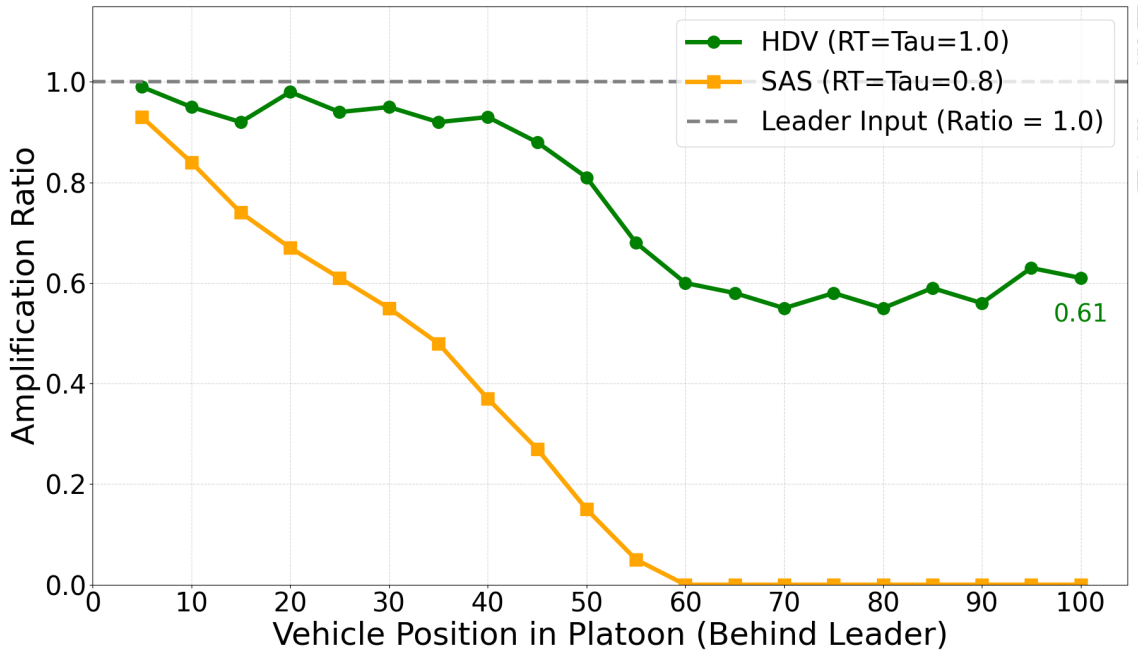

Figure 5.6: String stability analysis via perturbation amplification ratio. The green line (HDV) shows marginal stability with slow convergence, while the orange line (SAS) demonstrates rapid damping.

amplification ratio drops linearly and rapidly, reaching near-zero values by the 60th vehicle. This proves that the SAS actively absorbs the kinetic energy of the disturbance, ensuring that the braking maneuver of the n-th vehicle is always significantly milder than its predecessor.

5.4 Macroscopic Capacity Analysis

This section presents the results of the *virtual bottleneck* experiment, quantifying the maximum sustainable road capacity under saturated conditions. Based on the parameter modifications defined in Chapter 4, we evaluate three distinct scenarios:

1. **HDV Baseline (Green Line):** Represents current reality. Drivers in the bottleneck zone exhibit increased reaction times ($t_{reac} = 1.2$ seconds) and asymmetric risk perception ($C_{decel} = 1.8, C_{acc} = 0.75$).

doi:10.6342/NTU202600337

2. **SAS Takeover-Ready (Blue Line):** The proposed "safety-first" implementation. While the system utilizes the ideal configuration ($t_{reac} = 0.8$ seconds, $\tau = 0.8$ seconds) in open road sections to maximize efficiency, it explicitly adopts a conservative setting ($t_{reac} = 1.0$ second, $\tau = 1.0$ second) within the bottleneck zone to facilitate potential human takeover.

3. **SAS Robust (Orange Dashed Line):** The "ideal" implementation. It assumes full machine reliance without handover concerns, maintaining aggressive parameters ($t_{reac} = 0.8$ seconds, $\tau = 0.8$ seconds).

5.4.1 Fundamental Diagram Analysis

Figure 5.7 illustrates the flow-density relationship as traffic demand increases from 1600 veh/h to 2600 veh/h.

- **HDV Saturation (Green):** The baseline scenario saturates prematurely. The maximum capacity peaks at approximately **1638 veh/h** at a low input demand. Beyond this point, the flow becomes unstable and degrades to a discharge rate of $\approx 1488 - 1560$ veh/h. This confirms that human hesitation in confined environments is the primary bottleneck.

- **SAS Take-over Ready (Blue):** The proposed system demonstrates a clear capacity extension. The flow increases linearly with demand, reaching a peak of **1998 veh/h** at an input of 2100 veh/h. However, beyond this critical density, the flow breaks down and converges towards the HDV baseline (≈ 1494 veh/h), indicating the physical limit of the 1.0 second headway policy.

- **SAS Robust (Orange):** With aggressive parameters, the system delays the break-

doi:10.6342/NTU202600337

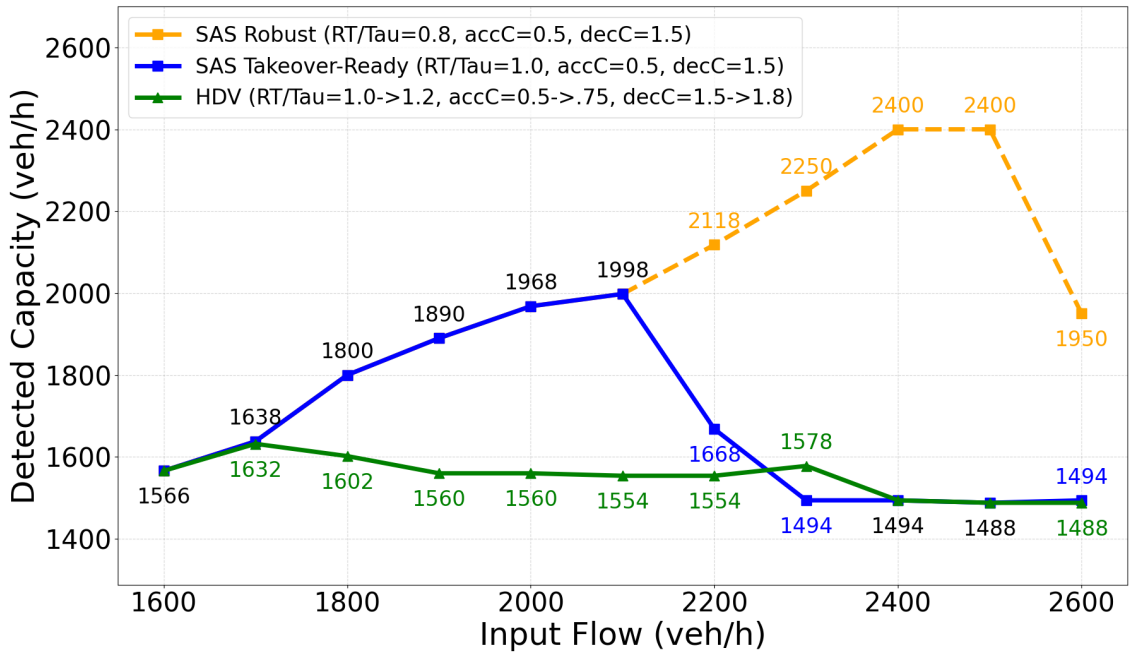

Figure 5.7: Capacity Comparison: HDV (Green), SAS Takeover-Ready (Blue), and SAS Robust (Orange). The Blue line represents the realistic capacity gain under takeover-ready safety constraints.

Table 5.1: Comparison of Macroscopic Road Capacity and Improvement Rates

Scenario	Configuration (Zone)	Peak Capacity	Improvement vs. HDV
HDV (Baseline)	$RT = 1.2s, \tau = 1.2s$	1638 veh/h	-
SAS Takeover-Ready	$RT = 1.0s, \tau = 1.0s$	**1998 veh/h**	**+21.98%**
SAS Robust	$RT = 0.8s, \tau = 0.8s$	**2400 veh/h**	**+46.52%**

down significantly, achieving a theoretical maximum of **2400 veh/h**. This represents the upper bound of infrastructure efficiency if handover safety margins were not a constraint.

5.4.2 Capacity Improvement Quantification

Table 5.1 summarizes the peak capacities and the percentage improvements relative to the HDV baseline.

The results highlight a crucial trade-off: adopting the **safety-aware takeover-ready** strategy secures a substantial **22%** capacity gain, whereas pushing for the theoretical limit

doi:10.6342/NTU202600337

could yield **46.5%**. The 22% gain is achieved purely by normalizing the driving behavior, even without aggressive gap reductions.

5.4.3 Mechanism of Improvement and Breakdown

The phenomenon observed in Figure 5.7 can be explained by two key mechanisms:

1. Normalization of Risk Perception

The primary reason the **SAS takeover-ready** outperforms the HDV—despite using similar temporal parameters (1.0 second vs 1.2 seconds)—is the elimination of **asymmetric behavioral hysteresis**. HDV drivers brake hard ($C_{decel} = 1.8$) but accelerate slowly ($C_{acc} = 0.75$), causing gaps to widen unnecessarily. The SAS maintains consistent logic ($C = 1.5/0.5$), ensuring that gaps created by departing vehicles are filled promptly, thus sustaining higher flow.

2. The Breakdown Threshold

The sharp drop in the Blue line after 2100 veh/h input illustrates the **density limit**. With a time headway of $\tau = 1.0$ second, the minimum safe distance is larger than that of $\tau = 0.8$ seconds. When the input flow exceeds the physical space allowed by a 1.0-second gap, the system is forced to decelerate to maintain safety, triggering a breakdown that cascades back to HDV levels. This confirms that while SAS optimizes flow stability, the absolute capacity is mathematically bounded by the chosen safety headway (τ).

5.4.4 Sensitivity Analysis: Impact of Reaction Time on Capacity

The previous section demonstrated the capacity improvements using specific reaction time configurations with 0.8 seconds for aggressive system and 1.0 second for takeover-

doi:10.6342/NTU202600337

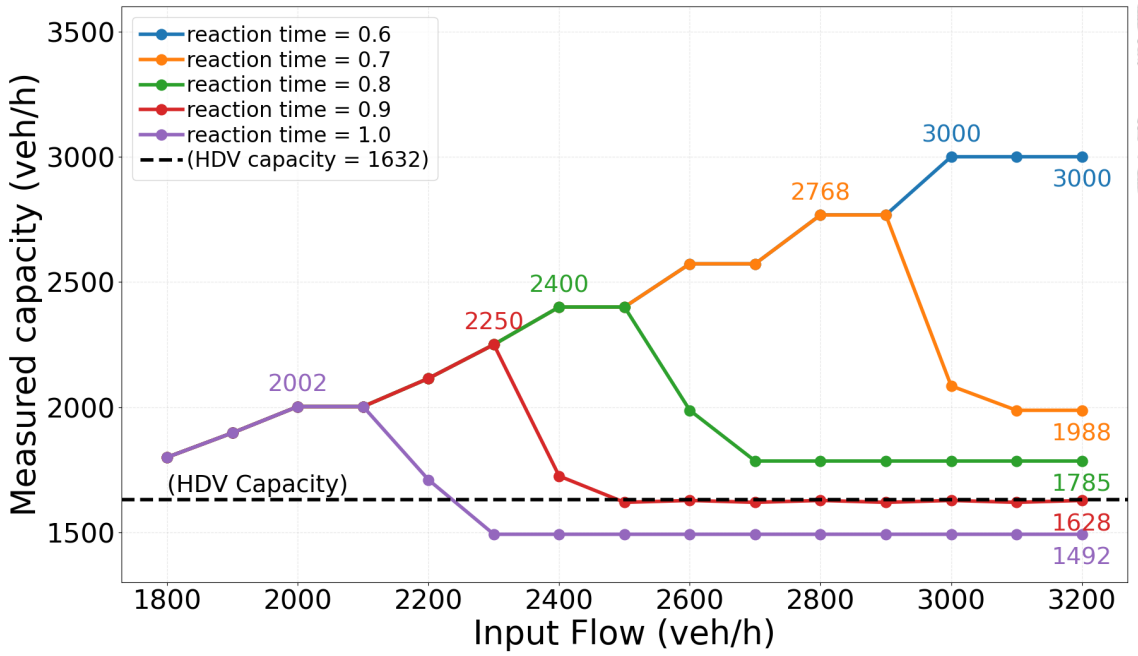

Figure 5.8: Sensitivity analysis of bottleneck capacity under varying SAS reaction times ($0.6s - 1.0s$). The black dashed line represents the baseline HDV capacity ($1632\ veh/h$). Even at a human-equivalent reaction time of 1.0s (purple line), the SAS achieves a peak capacity of $2002\ veh/h$, confirming that the elimination of perception error contributes significantly to flow efficiency.

ready situation. To generalize these findings and rule out the concern that the benefits are solely derived from aggressive parameter tuning, we conducted a sensitivity analysis on the SAS reaction time (t_{reac}^{SAS}).

Figure 5.8 illustrates the variation in bottleneck capacity as the reaction time degrades from the ideal 0.6 seconds to the human-level 1.0 second. Note that in this experiment, the time headway τ is coupled with reaction time ($\tau = t_{reac}^{SAS}$) to strictly satisfy string stability conditions.

The results, as shown in Figure 5.8, reveal a decisive advantage of the proposed system architecture:

- **Efficiency at Human-Level Latency:** The purple line represents the scenario where the SAS operates with a reaction time of 1.0 second, identical to the human baseline.

doi:10.6342/NTU202600337

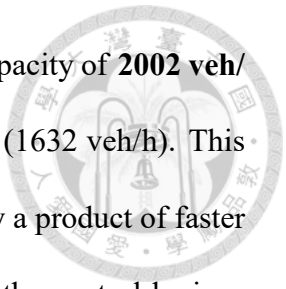

Despite this conservative latency, the system achieves a peak capacity of **2002 veh/h**, representing a **22.7% improvement** over the HDV baseline (1632 veh/h). This empirical evidence confirms that the capacity gain is not merely a product of faster reaction times but is fundamentally driven by the *precision* of the control logic—specifically, the elimination of stochastic perception errors ($k = 0$) and asymmetric hysteresis.

- **Latency-Dependent Breakdown Threshold:** The analysis also identifies the physical limits of the system. While the 0.6-second configuration sustains stability up to an input flow of 3000 veh/h, the 1-second configuration breaks down earlier at 2100 veh/h. This indicates that while "slow but precise" control is sufficient to improve capacity, "fast and precise" control is required to maximize the critical density and delay the onset of congestion under extreme demand.

This sensitivity analysis reinforces the validity of the capacity gains presented in Section 5.4.2, proving that the SAS remains a superior solution to human driving even under conservative operational constraints.

5.5 Sensitivity Analysis: Penetration Rate

To assess the feasibility of the SAS in a transitional mixed-autonomy environment, we evaluated the performance of the system across varying market penetration rate. To ensure statistical robustness and account for the stochastic nature of traffic generation and driver behavior, all results presented in this section are the **average of 10 simulation runs**. This rigorous testing reveals the performance stability of the system while eliminating

doi:10.6342/NTU202600337

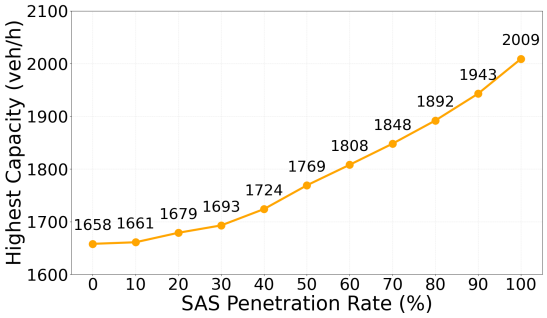

(a) Capacity Improvement

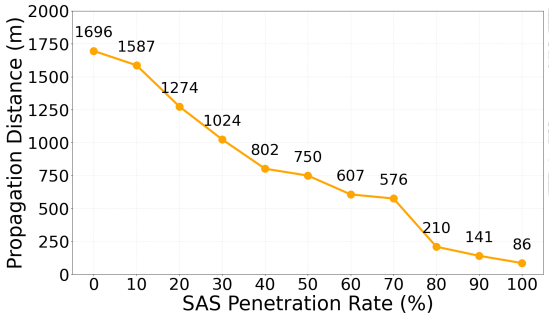

(b) Shockwave Propagation Distance

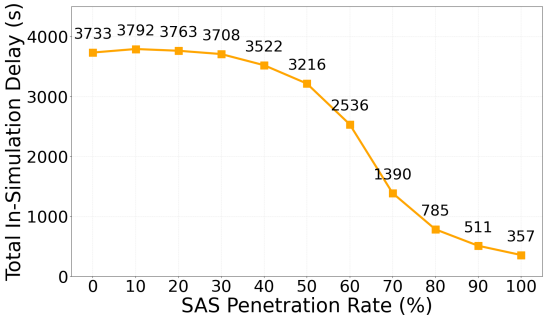

(c) Total Delay Reduction

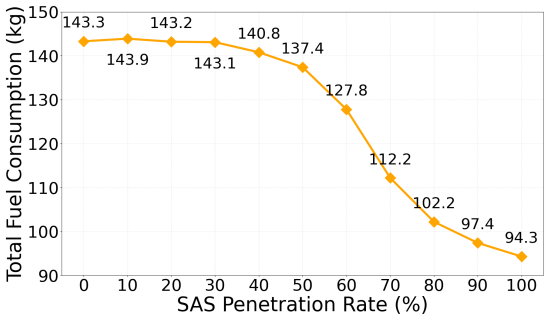

(d) Total Fuel Consumption

Figure 5.9: Macroscopic performance metrics under varying SAS penetration rates (0%-100%). The "Critical Mass" phenomenon is consistently observed between 50% and 80% across all efficiency metrics.

outliers. The analysis focuses on four key dimensions: macroscopic capacity, microscopic stability, total delay time and fuel consumption.

5.5.1 Quantitative Improvements

Figure 5.9 illustrates the trends for bottleneck capacity, shockwave propagation distance, total delay time, and fuel consumption based on the 10-seed average data. The improvements exhibit distinct, non-linear behaviors depending on the adoption phase:

- **Bottleneck Capacity (Figure 5.9a): Threshold-based growth.** The capacity improvement demonstrates a clear non-linear growth pattern. In the low-penetration range from 0% to 30%, the capacity remains relatively stagnant. A significant upward trend emerges only after exceeding the 30-40% threshold. As penetra-

doi:10.6342/NTU202600337

tion reaches 50% and above, the capacity grows quadratically, reaching a peak of 2009 veh/h at 100% penetration, representing a total improvement of approximately 21.2% over the baseline.

- **Shockwave Propagation Distance (Figure 5.9b): Early stability benefit.** In strong contrast to capacity, the stability benefit appears immediately upon deployment. With just 20% SAS penetration, the propagation distance drops significantly to 1274 meters with a reduction of 24.9%. The decline continues steadily, dropping to 86 meters at 100% penetration. This confirms that even a small proportion of SAS vehicles can act as effective "wave breakers", dampening oscillations well before macroscopic capacity benefits are fully realized.

- **Total Delay Time (Figure 5.9c): The efficiency gap and critical mass.** The delay analysis reveals a "deployment valley" in the early stages from 0-30%, where total delay exhibits negligible improvement. A decisive tipping point occurs between 40% and 60% penetration. The most dramatic reduction occurs at 70%, eventually reaching a minimum of 357 seconds at full adoption, confirming that a critical mass of approximately 50% is required to unlock significant travel time savings.

- **Fuel Consumption (Figure 5.9d): Sustainability and damping.** Finally, the fuel consumption analysis introduces the dimension of sustainability. The system achieves a remarkable 41.9% reduction in total fuel consumption at full adoption , dropping from 143.32 kg to 94.31 kg. The trend closely mirrors the delay reduction curve, with the most precipitous drop occurring between 50% and 80% penetration. This correlation confirms that the SAS improves efficiency fundamentally by suppressing traffic oscillations , thereby converting the kinetic energy usually lost in frequent braking maneuvers into sustained forward momentum.

doi:10.6342/NTU202600337

Table 5.2: Key Performance Metrics across Representative Penetration Rates (0-100%)

MPR	Bottleneck Capacity (veh/h)	Imp.(%)	Propagation Dist. (m)	Imp.(%)	Total Delay (s)	Imp.(%)	Fuel Consumption (kg)	Imp.(%)
0% (HDV)	1658	-	1696	-	3733	-	143.32	-
30%	1693	+2.1%	1024	-39.6%	3708	-0.7%	143.11	-0.2%
50%	1769	+6.7%	750	-55.8%	3216	-13.9%	137.42	-2.5%
80%	1892	+14.1%	210	-87.6%	785	-79.0%	102.20	-34.7%
100% (SAS)	2009	+21.2%	86	-94.9%	357	-90.4%	94.31	-41.9%

Note: The system performance evolves through three distinct phases:

- **30% (Stability Phase):** Offers significant safety gains (shockwave damping) despite marginal efficiency improvements.
- **50% (Critical Mass):** Represents the tipping point where delay and fuel consumption begin to drop sharply.
- **80% (High Efficiency):** System dominance is achieved, and stop-and-go oscillations are fully suppressed.

5.5.2 Interpretative Summary: The Phases of Deployment

Based on the quantitative milestones identified in Table 5.2, the deployment of SAS can be characterized by four distinct operational regimes defined by the breakpoints at **30%, 50%, and 80%**:

1. **Phase 1: Stability Precedes Efficiency**

   In the early adoption phase from 0% to 30%, the system functions primarily as a safety mechanism. While macroscopic efficiency metrics remain stagnant, the *shockwave propagation distance* is already reduced by nearly 40% at the 30% mark. This indicates that sparse SAS vehicles act as local "dampers," absorbing high-frequency oscillations to prevent rear-end collision risks, even if they are insufficient to accelerate the overall traffic stream.

2. **Phase 2: The Efficiency Gap**

   This phase ranging from 30% to 50% represents a "deployment valley." Despite

doi:10.6342/NTU202600337

improved stability, the *total delay* and *fuel consumption* exhibit a lag, improving only marginally until the 50% threshold is crossed. This suggests that below 50% penetration, the heterogeneity of the traffic stream prevents the formation of continuous, long-range platoons. The SAS vehicles are often trapped between HDVs, limiting their ability to regulate the aggregate flow speed.

3. **Phase 3: Critical Mass and Rapid Gain**

   The interval between 50% and 80% is the decisive "High-gain regime." Once the majority of vehicles are equipped, the probability of V2X coupling dominates. We observe the steepest descent in both *total delay*, dropping from 3216 seconds to 785 seconds, and *fuel xonsumption*. This confirms that **50% penetration is the critical tipping point** required to unlock thermodynamic efficiency and time savings.

4. **Phase 4: System Dominance**

   Beyond 80%, the system enters a saturation phase where it dictates the flow dynamics completely. The "stop-and-go" waves are virtually eliminated with less than 210 meters left. While further gains are achieved up to 100%, the transition from 80% to 100% represents the final optimization rather than a structural change in traffic behavior.

5.5.3 Damping Effect Analysis

To understand the mechanism behind these improvements, we analyzed the *perturbation amplification ratio* for different penetration rates. Figure 5.10 illustrates the evolution of the amplification ratio as the shockwave propagates through the platoon.

As shown in Figure 5.10, the 0% red line and 25% orange line scenarios exhibit weak stability, with ratios remaining high (> 0.6) even at the tail of the platoon. However, as

doi:10.6342/NTU202600337

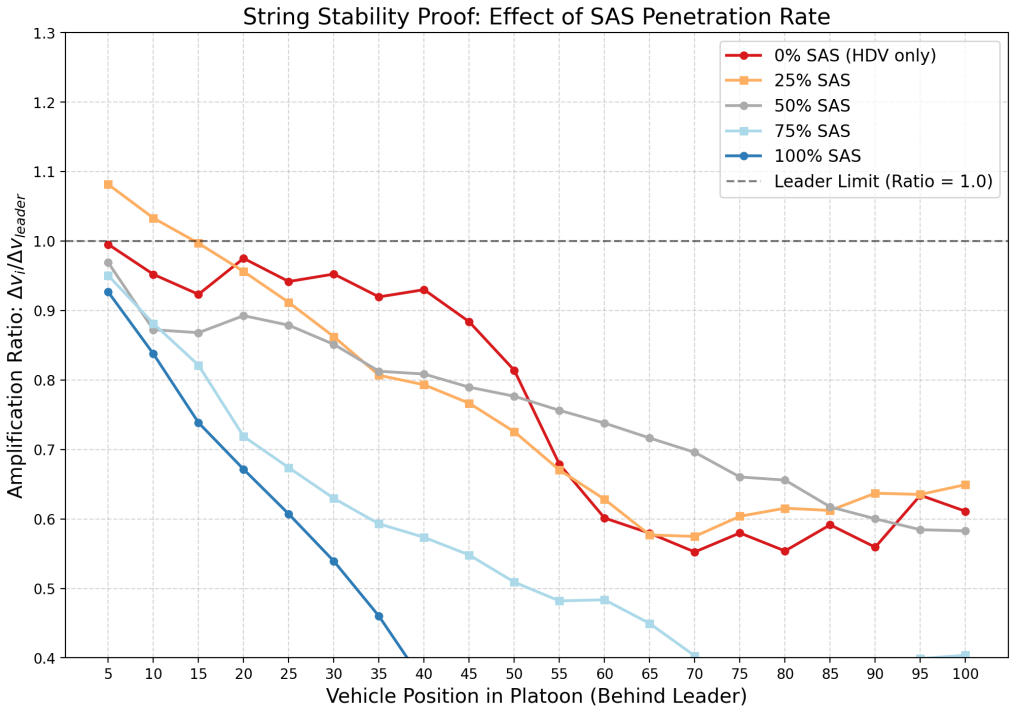

Figure 5.10: Damping Effect across Penetration Rates. The y-axis represents the amplification ratio ($\Delta v_i/\Delta v_{leader}$). A steeper downward slope indicates stronger shockwave absorption.

penetration increases to 100%, indicated by blue line, the curve drops sharply, confirming that a higher density of SAS vehicles creates a stronger "damping network" that rapidly absorbs kinetic energy.

5.5.4 Visual Verification: Shockwave Propagation

Finally, the mitigation of the shockwave is visualized using space-time diagrams in Figure 5.11. The red dashed line marks the **Shockwave Front**, representing the upstream limit of the congestion.

- **0% Penetration (Figure 5.11a):** The shockwave propagates deeply upstream, penetrating through more than half of the platoon. As the wavefront traverses the series of green HDV trajectories, it exhibits minor stochastic oscillations induced by perception noise yet shows no significant attenuation or damping effect. The distur-

doi:10.6342/NTU202600337

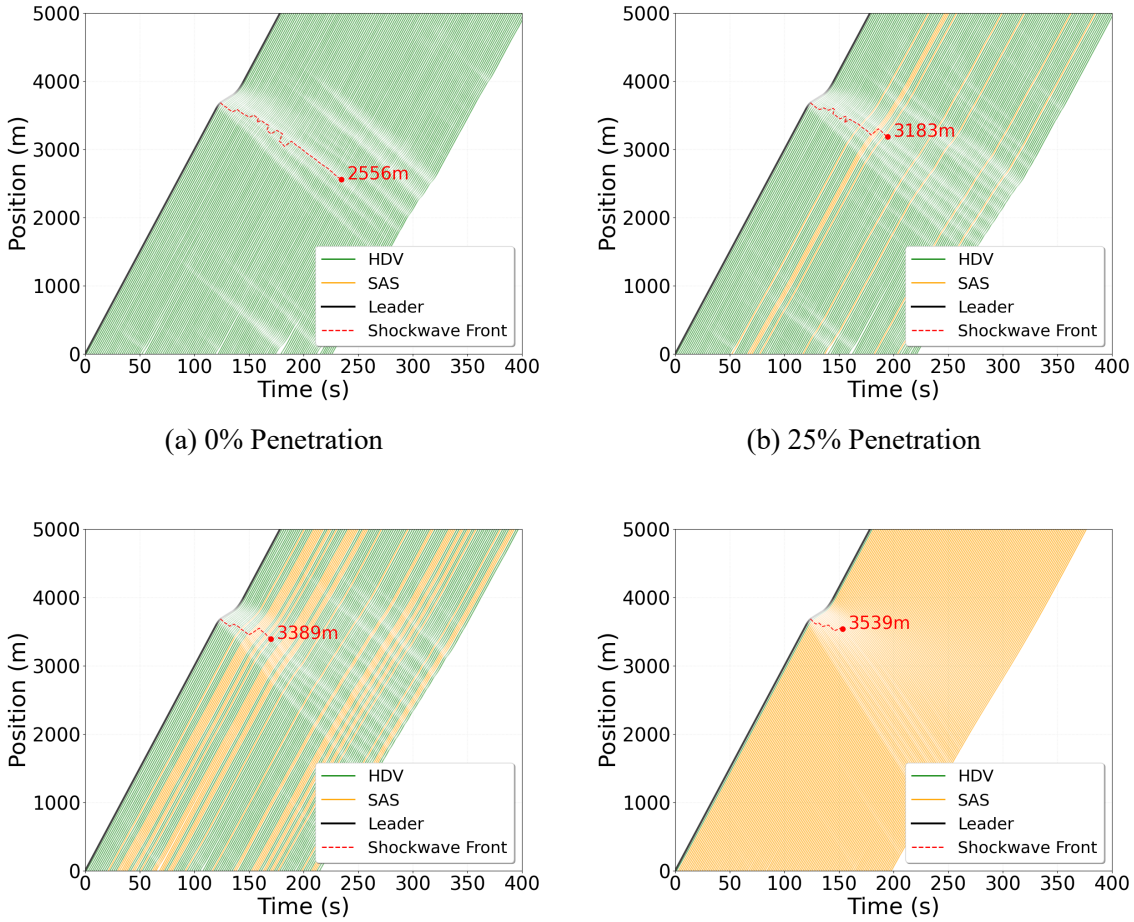

(a) 0% Penetration

(b) 25% Penetration

(c) 50% Penetration

(d) 100% Penetration

Figure 5.11: Space-Time Diagrams illustrating shockwave propagation at varying penetration rates. Green lines represent HDVs, while Orange lines represent SAS vehicles. The Red Dashed Line highlights the shockwave front. The shockwave front starts at the position of 3684 m.

doi:10.6342/NTU202600337

bance persists until reaching the position of 2556 meter, resulting in a total upstream propagation distance of **1128 meters**.

- **25% Penetration (Figure 5.11b):** The introduction of SAS vehicles, indicated by orange trajectories, initiates the mitigation of the disturbance. A notable observation occurs when the shockwave encounters **consecutive SAS vehicles**, where the red dashed line depicting the shockwave front is deflected towards the upper right. This trajectory shift indicates that the oscillation energy is partially absorbed by the optimized damping of the SAS. Consequently, the upstream propagation is curtailed earlier than in the baseline scenario, with the shockwave terminating at the position of **3183 meter**.

- **50% Penetration (Figure 5.11c):** The presence of SAS vehicles begins to break the continuous braking chain. The shockwave front becomes fragmented, and the propagation distance is noticeably reduced when coming across consecutive SAS vehicles, decreasing to only **295 meters**, which shortens the distance by 73.8%.

- **100% Penetration (Figure 5.11d):** The shockwave is immediately absorbed by the SAS vehicles following the initial deceleration of the leader, stopping at the position of 3539 meter, and propagating only a length of **145 meters**.

5.6 Impact of Network Reliability

Reliable V2V communication is critical for the safety of cooperative systems. This section evaluates the robustness of the SAS under realistic, unstable network conditions using the **Gilbert-Elliot Model**. To simulate a challenging environment, the average burst

doi:10.6342/NTU202600337

length is fixed at **15.0** ($L_{burst} = 15$), representing scenarios where packet losses occur in long, consecutive clusters. The packet loss rate is incrementally increased from 0.0 to 1.0.

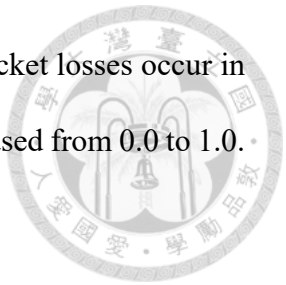

5.6.1 The Peril of Blind Estimation

First, we examine the system performance relying solely on the "constant velocity" state estimation without any timeout mechanism. As shown in Figure 5.12 (a), while the estimator is overly optimistic and maintains artificially high capacity ($\approx$ 2000 veh/h), it leads to a catastrophic rise in collision counts peaking at 21 collisions, indicating a "phantom robustness."

5.6.2 Robustness via Fail-Safe Mechanism

To mitigate the collision risks observed above, the fail-safe mechanism defined in Section 3.6.4 is activated. As modeled, this introduces a realistic compound latency of 2.5 seconds before human intervention becomes effective. Figure 5.12 (b) demonstrates the impact of introducing the **fail-safe mechanism**. The most critical improvement is safety—collision count is reduced to zero across the entire spectrum. The capacity curve exhibits a "graceful degradation" characteristic, gradually converging towards the HDV baseline as the network deteriorates.

5.7 Two-Lane Capacity with Lane Changing Analysis

This section analyzes the system performance in the realistic *two-lane highway scenario* defined in Chapter 4. Unlike the single-lane tests, this environment introduces **speed geterogeneity** to induce frequent lane-changing maneuvers. These maneuvers typically act as capacity-reducing disturbances, as human drivers often over-brake when cut off.

doi:10.6342/NTU202600337

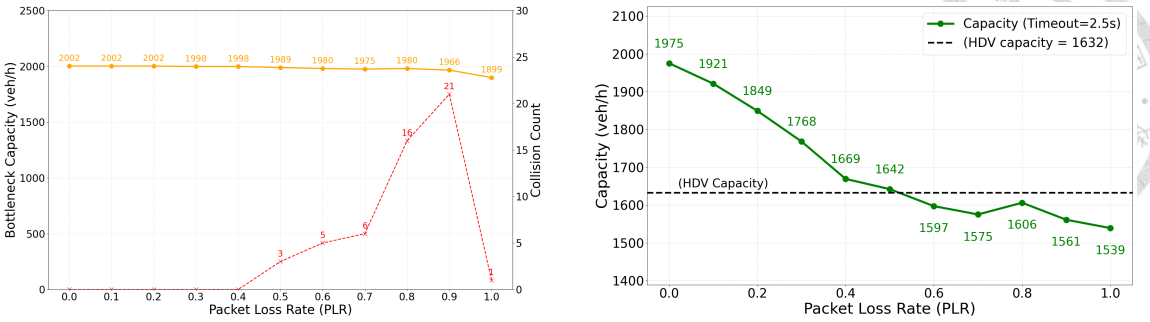

(a) No Fail-Safe (Zero-Accel Belief)

(b) With Fail-Safe Mechanism

Figure 5.12: Impact of network instability ($L_{burst} = 15$) on capacity and safety. (a) Without fail-safe, collisions skyrocket. (b) With fail-safe, collisions are eliminated, and capacity degrades gracefully. The black dashed line represents the baseline capacity (1632 veh/h) when the traffic consists entirely of Human-Driven Vehicles (HDVs).

Performance under Increasing Demand

Figure 5.13 (a) illustrates the detected flow rate against increasing input demand across different penetration rates.

- **HDV Baseline (0%, Blue Line):** The capacity saturates early at **2254 veh/hr**. The curve flattens quickly, indicating that human drivers struggle to maintain flow efficiency amidst the frequent cut-in disturbances caused by lane changers.
- **SAS Improvement:** As the SAS penetration increases, the saturation point is consistently pushed higher. At **100% penetration**, the system supports a massive flow of **4697 veh/hr**, effectively **doubling (+108%)** the capacity compared to the baseline.

Correlation between Penetration and Capacity

Figure 5.13 (b) extracts the maximum capacity peak for each penetration level. The results reveal a **strong linear positive correlation**. Unlike the bottleneck scenario where benefits might plateau, the two-lane scenario shows continuous gains ($2254 \rightarrow 2863 \rightarrow$

doi:10.6342/NTU202600337

$3514 \rightarrow 4166 \rightarrow 4697$). This suggests that SAS does not just reduce headway; it fundamentally stabilizes **lateral interactions**. Under SAS guidance, vehicles can execute and accommodate lane changes more **decisively and tightly**. The reduced reaction time allows followers to accept cut-ins without triggering the severe "stop-and-go" shockwaves that typically cripple HDV traffic.

5.8 Discussion

The experimental results presented in this chapter demonstrate the multi-faceted benefits of the SAS. Beyond the raw performance metrics, this section synthesizes the findings to discuss the underlying mechanisms, the inherent trade-offs between safety and efficiency, and the broader implications for mixed autonomy deployment.

5.8.1 Linking Microscopic Stability to Macroscopic Capacity

A key contribution of this study is the empirical verification of the link between string stability and road capacity. The *pulse step* tests (Section 5.3) revealed that the SAS acts as a **low-pass filter**, attenuating high-frequency braking oscillations. Macroscopically, this damping effect prevents the formation of "phantom jams" at bottlenecks. As observed in the fundamental diagram (Section 5.4), the capacity drop in HDV traffic is triggered by the *amplification* of minor speed variances. By suppressing these variances at the individual vehicle level, the SAS effectively postpones the flow breakdown, allowing the bottleneck to operate at a higher density state, with the increase from 1632 to 1998 veh/h, before saturation occurs. This confirms that **homogenizing flow dynamics** is as critical as reducing time headways for capacity enhancement.

doi:10.6342/NTU202600337

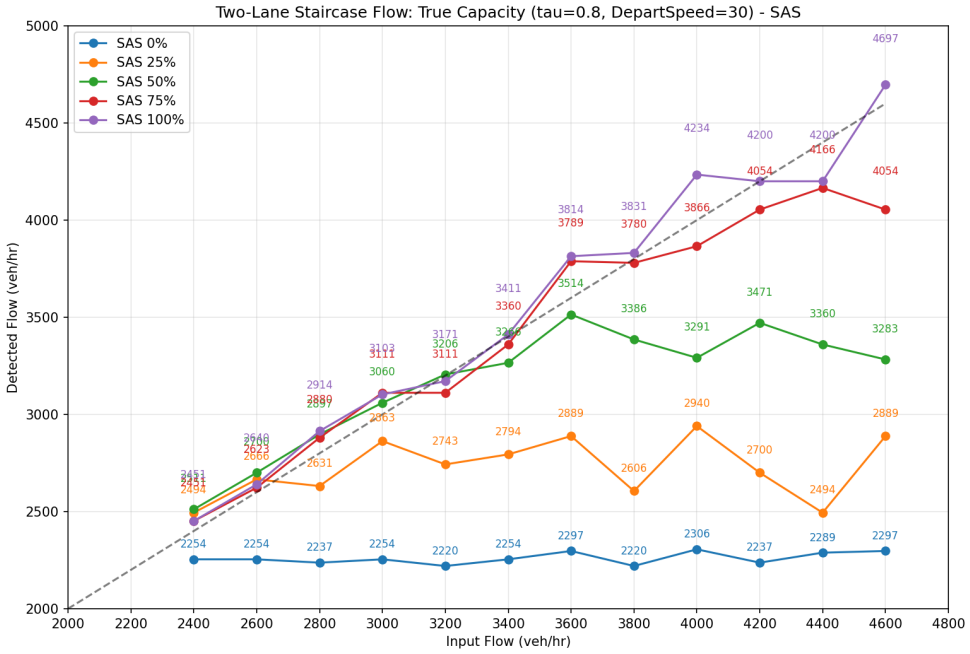

(a) Detected Flow vs. Input Demand across Penetration Rates.

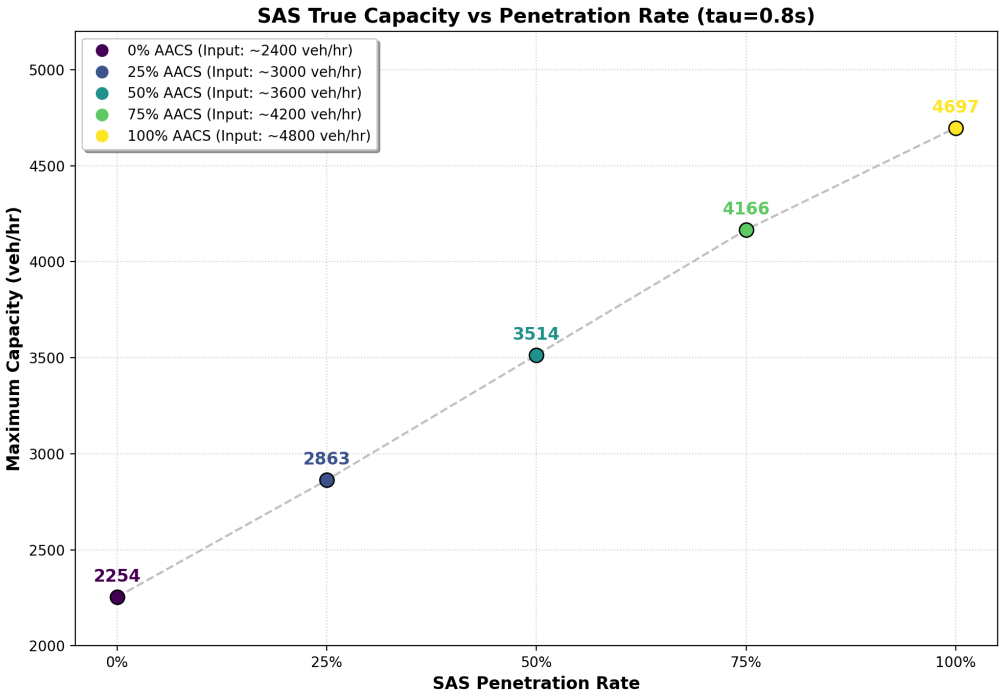

(b) Maximum Capacity vs. SAS Penetration Rate.

Figure 5.13: Two-Lane Scenario Results. (a) The system maintains flow stability at much higher densities than HDVs. (b) Capacity improves linearly, demonstrating that SAS effectively mitigates the capacity loss usually caused by lane-changing disturbances.

doi:10.6342/NTU202600337

5.8.2 The Trade-off between Handover Safety and Maximum Efficiency

The comparison between the "SAS take-over ready" and "SAS Robust" scenarios highlights a fundamental design trade-off. While the theoretical limit of the system promises a massive 46% capacity gain, the practical necessity of maintaining a *takeover-ready* buffer constrains the realizable gain to approx. 22%. This *safety insurance* is unavoidable in Level 2/3 systems where the human driver remains the ultimate fallback. However, our results suggest that even with this constraint, the system provides substantial value. The elimination of human reaction latency and asymmetry (C_{decel} vs C_{acc}) alone contributes significantly to flow smoothing, proving that **behavioral regularization** yields benefits independent of aggressive gap reduction.

5.8.3 Phased Evolution of System Benefits

The sensitivity analysis indicates that the operational benefits of the SAS evolve through three distinct phenomenological phases rather than scaling linearly. During the initial stage of 0% to 30% penetration, the system exhibits a decoupled improvement profile where shockwave damping improves significantly while traffic efficiency remains stagnant. The intermediate interval between 30% and 50% functions as a transitional tipping point, where the increasing density of consecutive SAS vehicles begins to convert stability gains into measurable reductions in travel delay. Finally, as penetration exceeds 50%, the traffic flow enters a state of operational dominance, characterized by the effective eradication of stop-and-go waves and a non-linear surge in total roadway capacity. In summary, the deployment strategy must be adaptive: prioritizing safety messaging in the short term, aggressive incentives in the medium term to reach critical mass, and efficiency

doi:10.6342/NTU202600337

maximization in the long term.

doi:10.6342/NTU202600337

Chapter 6

Conclusion

6.1 Summary of Work

This thesis addressed the critical challenge of traffic congestion caused by stop-and-go shockwaves in a mixed autonomy environment. Recognizing that human reaction latency and perception errors—governed by **Hick's Law** and **Weber's Law**—are the primary causes of string instability, we proposed SAS.

The SAS is not merely a driver assistance tool but a mechanism designed to **transform the driving task from a high-latency Choice Reaction Time (CRT) paradigm to a low-latency Simple Reaction Time (SRT) paradigm**. By leveraging V2X communication to provide preemptive, numeric advisories, the system effectively bypasses the complex cognitive processing stages of human drivers.

To ensure a realistic evaluation, we developed HCCFM within the SUMO simulation environment. By incorporating Weber's Law for perception error, the model successfully replicated the instability characteristics of real-world traffic, serving as a rigorous baseline for testing the proposed system.

doi:10.6342/NTU202600337

6.2 Key Findings

The comprehensive evaluation yielded several significant findings regarding the effectiveness and characteristics of the SAS:

1. **Microscopic Damping Effect:** The system reduced the shockwave propagation distance by 94.9%, confirming that the SAS converts the traffic stream from a marginally stable state to a **strictly stable state**, effectively acting as a low-pass filter for disturbances.

2. **Macroscopic Capacity Enhancement:** The SAS demonstrated a significant increase in road capacity, representing a 22.4% improvement while maintaining a conservative "takeover-ready" state. This demonstrates that substantial efficiency gains are achievable purely by normalizing driving behavior and eliminating human asymmetry, even when the system is constrained to human-like safety margins to ensure seamless manual handover.

3. **Phased Benefit Realization — Non-linear Scalability and Critical Mass:** The sensitivity analysis reveals that the benefits of the syste do not scale linearly with market penetration. While initial deployment up to 30% MPR primarily enhances string stability and safety by dampening shockwaves, significant improvements in traffic efficiency—such as reduced delays and increased bottleneck capacity—only materialize after crossing a critical mass threshold of approximately 50%. This finding indicates that while immediate safety benefits can be realized with low adoption, achieving the full potential of flow harmonization requires policy interventions to push adoption rates beyond this tipping point.

doi:10.6342/NTU202600337

4. **Robustness and Fail-Safe:** The system demonstrated robustness against network instability. The proposed fail-safe mechanism, which reverts to a conservative human driving mode during communication blackouts, ensured zero collisions even under high packet loss rates, achieving a graceful degradation of performance.

6.3 Limitations

While the results are promising, several limitations of this study must be acknowledged:

1. **Driver Compliance Assumption:** The current simulation assumes that drivers comply 100% with the system advisories. In reality, driver trust, distraction, or resistance could lead to partial compliance, potentially reducing system effectiveness.

2. **Passenger Comfort (Jerk):** The study focused primarily on flow stability and safety. The rapid acceleration adjustments required to dampen shockwaves might result in high jerk values, which could negatively affect passenger comfort.

3. **Simplified Lateral Interactions:** Although a two-lane scenario was tested, the interaction between mandatory lane changes such as on-ramps and the longitudinal advisory logic requires further investigation.

4. **Sensor Noise and Latency in SAS:** This study assumes that the SAS-equipped vehicles possess near-perfect information accuracy ($\epsilon \approx 0$) via V2V/Sensors. In physical deployment, ToF sensors have their own noise profiles and processing delays, which were simplified in this simulation.

doi:10.6342/NTU202600337

5. **Vehicle Heterogeneity:** The current simulation models a homogeneous fleet of passenger cars. The impact of heavy vehicles such as trucks and buses with different dynamic capabilities on the advisory logic remains to be explored.

6.4 Future Work

Future research directions to extend this work include:

1. **Incorporating a Compliance Model:** Introducing a stochastic compliance factor to model the probability of a driver ignoring or delaying the execution of an advisory, allowing for more realistic performance bounds.

2. **Comfort-Aware Control:** Optimizing the control algorithm to include a cost function for jerk, balancing the trade-off between shockwave suppression and ride comfort.

3. **Robustness against Sensor Uncertainty:** Extending the control algorithm to include Kalman Filtering or other state-estimation techniques to handle realistic sensor noise in the SAS input data.

4. **Heterogeneous Traffic Integration:** Adapting the advisory logic to account for diverse vehicle classes, potentially dynamically adjusting the safety headways based on the specific braking capabilities of the following vehicle.

5. **Field Operational Tests:** validating the proposed concepts using driving simulators or small-scale field tests with connected vehicles to assess real-human interaction with the advisory interface.

doi:10.6342/NTU202600337

In conclusion, this thesis demonstrates that the SAS is a viable and high-impact solution for the transitional period of mixed autonomy. By augmenting human capabilities rather than replacing them, SAS offers a practical path to alleviating highway congestion before the full advent of autonomous driving.

doi:10.6342/NTU202600337

References

[1] Y. Sugiyama, M. Fukui, M. Kikuchi, K. Hasebe, A. Nakayama, K. Nishinari, S.-i. Tadaki, and S. Yukawa, "Traffic jams without bottlenecks—experimental evidence for the physical mechanism of the formation of a jam," *New Journal of Physics*, vol. 10, no. 3, p. 033001, mar 2008.

[2] M. Barth and K. Boriboonsomsin, "Real-world carbon dioxide impacts of traffic congestion," *Transportation Research Record*, vol. 2058, no. 1, pp. 163–171, 2008.

[3] P. A. Lopez, M. Behrisch, L. Bieker-Walz, J. Erdmann, Y.-P. Flötteröd, R. Hilbrich, L. Lücken, J. Rummel, P. Wagner, and E. Wießner, "Microscopic traffic simulation using sumo," in *The 21st IEEE International Conference on Intelligent Transportation Systems*. IEEE, 2018.

[4] B. Heydecker and J. Addison, "Analysis and modelling of traffic flow under variable speed limits," *Transportation Research Part C: Emerging Technologies*, vol. 19, no. 2, pp. 206–217, 2011, emerging theories in traffic and transportation and methods for transportation planning and operations. [Online]. Available: https://www.sciencedirect.com/science/article/pii/S0968090X10000926

[5] M. Papageorgiou, E. Kosmatopoulos, and I. Papamichail, "Effects of variable speed limits on motorway traffic flow," *Transportation Research Record*, vol. 2047, no. 1,

doi:10.6342/NTU202600337

pp. 37–48, 2008. [Online]. Available: https://doi.org/10.3141/2047-05

[6] A. Hegyi, S. Hoogendoorn, M. Schreuder, H. Stoelhorst, and F. Viti, "Specialist: A dynamic speed limit control algorithm based on shock wave theory," in *2008 11th International IEEE Conference on Intelligent Transportation Systems*, 2008, pp. 827–832.

[7] A. Ghiasi, O. Hussain, Z. S. Qian, and X. Li, "A mixed traffic capacity analysis and lane management model for connected automated vehicles: A markov chain method," *Transportation Research Part B: Methodological*, vol. 106, pp. 266–292, 2017.

[8] H. Abdulsattar, M. R. K. Siam, and H. Wang, "Characterisation of the impacts of autonomous driving on highway capacity in a mixed traffic environment: An agent-based approach," *IET Intelligent Transport Systems*, vol. 14, no. 9, pp. 1132–1141, 2020.

[9] M. Guériau and I. Dusparic, "Quantifying the impact of connected and autonomous vehicles on traffic efficiency and safety in mixed traffic," in *2020 IEEE 23rd International Conference on Intelligent Transportation Systems (ITSC)*. IEEE, 2020, pp. 1–8.

[10] M. Sala and F. Soriguera, "Capacity of a freeway lane with platoons of autonomous vehicles mixed with regular traffic," *Transportation Research Part B: Methodological*, vol. 147, pp. 116–131, 2021. [Online]. Available: https://www.sciencedirect.com/science/article/pii/S0191261521000540

doi:10.6342/NTU202600337

[11] J. Wang, Y. Zheng, C. Chen, Q. Xu, and K. Li, "Leading cruise control in mixed traffic flow: System modeling, controllability, and string stability," *IEEE Transactions on Intelligent Transportation Systems*, vol. 23, no. 8, pp. 12 861–12 876, 2022.

[12] C. Liu, F. Zheng, H. X. Liu, and X. Liu, "Optimizing mixed traffic flow: Longitudinal control of connected and automated vehicles to mitigate traffic oscillations," *IEEE Transactions on Intelligent Transportation Systems*, 2025, early Access.

[13] K. Li, J. Wang, and Y. Zheng, "Cooperative formation of autonomous vehicles in mixed traffic flow: Beyond platooning," *IEEE Transactions on Intelligent Transportation Systems*, vol. 23, no. 9, pp. 15 951–15 966, 2022.

[14] C. Wu, A. R. Kreidieh, K. Parvate, E. Vinitsky, and A. M. Bayen, "Flow: A modular learning framework for mixed autonomy traffic," *IEEE Transactions on Robotics*, vol. 38, no. 2, pp. 1270–1286, 2022.

[15] B. Chen, D. Sun, J. Zhou, W. Wong, and Z. Ding, "A future intelligent traffic system with mixed autonomous vehicles and human-driven vehicles," *Information Sciences*, vol. 529, pp. 59–72, 2020. [Online]. Available: https://www.sciencedirect.com/science/article/pii/S0020025520300736

[16] Y. Pan, Y. Wu, L. Xu, C. Xia, and D. L. Olson, "The impacts of connected autonomous vehicles on mixed traffic flow: A comprehensive review," *Physica A: Statistical Mechanics and its Applications*, vol. 635, p. 129454, 2024.

[17] W. J. Schakel, B. van Arem, and B. D. Netten, "Effects of cooperative adaptive cruise control on traffic flow stability," in *13th International IEEE Conference on Intelligent Transportation Systems*, 2010, pp. 759–764.

doi:10.6342/NTU202600337

[18] M. Di Vaio, G. Fiengo, A. Petrillo, A. Salvi, S. Santini, and M. Tufo, "Cooperative shock waves mitigation in mixed traffic flow environment," *IEEE Transactions on Intelligent Transportation Systems*, vol. 20, no. 12, pp. 4339–4353, 2019.

[19] M. Garg and M. Bouroche, "Can connected autonomous vehicles improve mixed traffic safety without compromising efficiency in realistic scenarios?" *IEEE Transactions on Intelligent Transportation Systems*, 2023.

[20] C. H. P. Nguyen, N. H. Hoang, S. Lee, and H. L. Vu, "A system optimal speed advisory framework for a network of connected and autonomous vehicles," *IEEE Transactions on Intelligent Transportation Systems*, vol. 23, no. 6, pp. 5727–5739, 2022.

[21] N. Wan, A. Vahidi, and A. Luckow, "Optimal speed advisory for connected vehicles in arterial roads and the impact on mixed traffic," *Transportation Research Part C: Emerging Technologies*, vol. 69, pp. 548–563, 2016. [Online]. Available: https://www.sciencedirect.com/science/article/pii/S0968090X16000292

[22] H.-P. Wu, W.-H. Shen, Y.-L. Wei, H.-M. Tsai, and Q. Xie, "Traffic shockwave mitigation with human-driven vehicles: is it feasible?" in *Proceedings of the First ACM International Workshop on Smart, Autonomous, and Connected Vehicular Systems and Services*, ser. CarSys '16. New York, NY, USA: Association for Computing Machinery, 2016, p. 38–43. [Online]. Available: https://doi.org/10.1145/2980100.2980101

[23] S. Krauß, "Microscopic modeling of traffic flow: Investigation of collision free vehicle dynamics," Ph.D. dissertation, Universität zu Köln, 1998, accessed: 2025-07-03.

doi:10.6342/NTU202600337

[24] M. Treiber, A. Hennecke, and D. Helbing, "Congested traffic states in empirical observations and microscopic simulations," *Physical Review E*, vol. 62, no. 2, p. 1805–1824, Aug. 2000. [Online]. Available: http://dx.doi.org/10.1103/PhysRevE.62.1805

[25] W.-X. Zhu and H. Zhang, "Analysis of mixed traffic flow with human-driving and autonomous cars based on car-following model," *Physica A: Statistical Mechanics and its Applications*, vol. 496, pp. 274–285, 2018.

[26] M. Alturki, N. Ratrout, S. M. Rahman, and I. Reza, "Impacts of autonomous vehicles on traffic flow characteristics under mixed traffic environment: Future perspectives," *Sustainability*, vol. 13, p. 11052, 10 2021.

[27] J. Sun, Z. Zheng, and J. Sun, "The relationship between car following string instability and traffic oscillations in finite-sized platoons and its use in easing congestion via connected and automated vehicles with idm based controller," *Transportation Research Part B: Methodological*, vol. 142, pp. 58–83, 2020.

[28] M. Treiber, A. Kesting, and D. Helbing, "Delays, inaccuracies and anticipation in microscopic traffic models," *Physica A: Statistical Mechanics and its Applications*, vol. 360, no. 1, pp. 71–88, 2006. [Online]. Available: https://www.sciencedirect.com/science/article/pii/S0378437105004395

[29] X. Li, Y. Xiao, X. Zhao, X. Ma, and X. Wang, "Modeling mixed traffic flows of human-driving vehicles and connected and autonomous vehicles considering human drivers' cognitive characteristics and driving behavior interaction," *Physica A: Statistical Mechanics and its Applications*, vol. 609, p. 128368, 2023. [Online]. Available: https://www.sciencedirect.com/science/article/pii/S0378437122009268

doi:10.6342/NTU202600337

[30] E. H. Weber, *De Tactu: Annotationes Anatomicae et Physiologicae*. Leipzig: Koehler, 1834.

[31] X.-Y. Guo, G. Zhang, and A.-F. Jia, "Study on mixed traffic of autonomous vehicles and human-driven vehicles with different cyber interaction approaches," *Vehicular Communications*, vol. 39, p. 100550, 2023. [Online]. Available: https://www.sciencedirect.com/science/article/pii/S2214209622000973

[32] M. Green, ""how long does it take to stop?" methodological analysis of driver perception-brake times," *Transportation Human Factors*, vol. 2, pp. 195–216, 09 2000.

[33] W. E. Hick, "On the rate of gain of information," *Quarterly Journal of Experimental Psychology*, vol. 4, no. 1, pp. 11–26, 1952.

[34] R. Hyman, "Stimulus information as a determinant of reaction time," *Journal of Experimental Psychology*, vol. 45, no. 3, p. 188, 1953.

[35] B. Coll-Perales, M. C. Lucas-Estañ, T. Shimizu, J. Gozalvez, T. Higuchi, S. Avedisov, O. Altintas, and M. Sepulcre, "End-to-end v2x latency modeling and analysis in 5g networks," *IEEE Transactions on Vehicular Technology*, vol. 72, no. 4, pp. 5094–5109, 2023.

[36] J. Erdmann and P. Wagner, "Sumo' s interpretation of the krauß model," Pre-print, SUMO User Conference, May 2025, pre-print version, accessed July 3, 2025. [Online]. Available: https://sumo.dlr.de/pdf/2025/pre-print-2638.pdf

[37] G. E. Uhlenbeck and L. S. Ornstein, "On the theory of the brownian motion," *Physical review*, vol. 36, no. 5, p. 823, 1930.

doi:10.6342/NTU202600337

[38] H. M. Zhang, "A mathematical theory of traffic hysteresis," *Transportation Research Part B: Methodological*, vol. 33, no. 1, pp. 1–23, 1999.

[39] H. Yeo and A. Skabardonis, "Understanding stop-and-go traffic in view of asymmetric traffic theory," in *Transportation and Traffic Theory 2009: Golden Jubilee*. Springer, 2009, pp. 99–115.

[40] U.S. Department of Transportation Federal Highway Administration, "Next generation simulation (NGSIM) vehicle trajectories and supporting data," Available: https://data.transportation.gov/Automobiles/Next-Generation-Simulation-NGSIM-Vehicle-Trajector/8ect-6jqj, 2016, accessed: Jan. 08, 2026.

[41] Freeway Bureau, MOTC, "Traffic information system: Historical data," [Online]. Available: https://tisvcloud.freeway.gov.tw/history-list.php, 2026, accessed: Jan. 08, 2026.

doi:10.6342/NTU202600337